

Constraining scalar-tensor theories by neutron star-black hole gravitational wave events

RUI NIU ^{1,2} XING ZHANG ^{1,2} BO WANG ^{1,2} AND WEN ZHAO ^{1,2}

¹*CAS Key Laboratory for Researches in Galaxies and Cosmology, Department of Astronomy, University of Science and Technology of China, Chinese Academy of Sciences, Hefei, Anhui 230026, China;*

²*School of Astronomy and Space Sciences, University of Science and Technology of China, Hefei 230026, China*

(Received; Revised; Accepted)

Submitted to

ABSTRACT

With the continuous upgrade of detectors, more and more gravitational wave (GW) events were captured by the LIGO Scientific Collaboration and Virgo Collaboration (LVC), which offers a new avenue to test General Relativity and explore the nature of gravity. Although, various model-independent tests have been performed by LVC in previous works, it is still interesting to ask what constraints on specific models can be placed by current GW observations. In this work, we focus on three models of scalar-tensor theories, the Brans-Dicke theory (BD), the theory with scalarization phenomena proposed by Damour and Esposito-Farèse (DEF), and Screened Modified Gravity (SMG). From all 4 possible NSBH events so far, we use two of them to place the constraints. The other two are excluded in this work due to the possible unphysical deviations. We consider the inspiral range with the cutoff frequency at the innermost stable circular orbit and add a modification of dipole radiation into the waveform template. The scalar charges of neutron stars in the dipole term are derived by solving the Tolman-Oppenheimer-Volkoff equations for different equations-of-states. The constraints are obtained by performing the full Bayesian inference with the help of the open source software *Bilby*. The results show that the constraints given by GWs are comparable with those given by pulsar timing experiments for DEF theory, but are not competitive with the current solar system constraints for BD and SMG theories.

Keywords: gravitational wave, scalar-tensor theory

1. INTRODUCTION

The theory of General Relativity (GR), as one of the two pillars of modern physics, is regarded as the most beautiful theory by common consent (Chandrasekhar 1984). The splendor of GR is not only due to its elegant mathematical expression, but also its precise consistency with experimental tests. Since Einstein proposed GR in 1915, a large number of experimental tests have been conducted, ranging from laboratory scale (Sabulsky et al. 2019; Hoyle et al. 2001; Adelberger 2001) to solar system scale (Will 2018, 2014) and to cosmological scale (Jain & Khoury 2010; Koyama 2016; Clifton et al. 2012). In recent years, pulsar timing experiments (Stairs

2003; Manchester 2015; Wex 2014; Kramer 2017) and gravitational wave observations (Abbott et al. 2019a; Collaboration et al. 2020; Abbott et al. 2016a, 2019b) provide great opportunities to test GR under strong field conditions. So far, all these experimental tests have supported GR at a very high level of accuracy.

Although great success has been achieved, there are still problems that GR cannot solve. At the theoretical level, GR has been facing difficulties such as the singularity and quantization problems (DeWitt 1967; Kiefer 2007). At the experimental level, to explain astrophysical and cosmological observation data within the GR framework, it is necessary to introduce the so-called dark matter and dark energy whose physical nature is still unknown, which might imply the incompleteness of GR (Cline 2013; Sahmi 2004). With the motivation to solve these problems, many modified gravity theories have been proposed. Among them, the scalar-tensor

60 theories are generally considered as a promising candi-
61 date (Yasunori Fujii 2016).

62 The origin of scalar-tensor theories can be traced back
63 to the works of Kaluza and Klein (Kaluza 1921; Klein
64 1926). The form that we are familiar with today was
65 developed by works (Brans & Dicke 1961; Fierz 1956;
66 Jordan 1955). The scalar-tensor theories have poten-
67 tial relations with dark energy, dark matter and infla-
68 tion, which continually arouse people’s interest in con-
69 temporary (Clifton et al. 2012; Barrow & ichi Maeda
70 1990; Burd & Coley 1991; Schimd et al. 2005; Kainu-
71 lainen & Sunhede 2006; Brax et al. 2006). We focus
72 on three different models of scalar-tensor theories in
73 this work, i.e., the Brans-Dicke theory (BD), the the-
74 ory with scalarization phenomena proposed by Damour
75 and Esposito-Farèse (DEF), and the screened modified
76 gravity (SMG). The theory of Brans and Dicke (Brans
77 & Dicke 1961) takes Mach’s principle as the starting
78 point, which tells the phenomenon of inertia depends on
79 the mass distribution of the universe. Thus the gravita-
80 tional constant is promoted to be variable and coupled to
81 the Einstein-Hilbert Lagrangian as a scalar field ¹. The
82 Brans-Dicke theory is the simplest scalar-tensor theory
83 and is usually seen as the prototype of scalar-tensor the-
84 ories, which has been well studied and constrained (Will
85 2018). Extensive tests have been performed in weak field
86 regimes based on parameterized post-Newtonian formal-
87 ism. The most stringent constrain is given by the mea-
88 surement of Shapiro time delay from Cassini-Huygens
89 spacecraft (Bertotti et al. 2003).

90 For Brans-Dicke theory, this tight bound requires
91 deviations from GR in all gravitational experiments
92 to be very small in both weak-field and strong-field.
93 However, in the works of Damour and Esposito-Farèse
94 (Damour & Esposito-Farèse 1993; Damour & Esposito-
95 Farese 1992), they showed that some nonperturbative
96 effects can emerge in strong-field conditions. When the
97 compactness of an object exceeds a critical point, a phe-
98 nomenon, so-called spontaneous scalarization, which is
99 usually discussed by analogy with the spontaneous mag-
100 netization in ferromagnets (Damour & Esposito-Farèse
101 1996), will arise. This phenomenon can make the behav-
102 ior in gravitational experiments involving compact ob-
103 jects, like binary neutron star systems, have remarkable
104 differences from the experiments in weak-field regimes.
105 In the models that can develop nonperturbative strong-
106 field effects, order-of-unity deviations from GR are still
107 allowed in strong-field experiments, under the premise

108 of passing the most stringent weak-field constraint. In
109 the subsequent researches, different kinds of scalariza-
110 tion phenomena, dynamical scalarization and induced
111 scalarization, are discovered in numerical relativity sim-
112 ulations of merging binary neutron stars evolution (Ba-
113 rousse et al. 2013). In binary neutron star systems, the
114 phenomenon that the scalar field produced by the scalar-
115 ized component can induce the scalarization of another
116 component which is not scalarized initially is called in-
117 duced scalarization. Since the GW event used in this
118 work is considered as a neutron star-black hole (NSBH)
119 binary event, this phenomenon is not needed to be con-
120 cerned. Dynamical scalarization is a phenomenon that a
121 binary system, in which both two components cannot be
122 scalarized in isolation, is triggered to scalarization due
123 to their gravitational binding energy of orbit. However,
124 in the previous works (Palenzuela et al. 2014; Sampson
125 et al. 2014), it has been shown that dynamical scalar-
126 ization is difficult to be detected by current detectors.
127 Therefore, we only consider spontaneous scalarization in
128 this work.

129 The nonperturbative strong-field effects can be con-
130 strained by pulsar timing experiments (Damour &
131 Esposito-Farèse 1998, 1996). Because of precise mea-
132 surement technology and decades of data accumulation,
133 the orbital period decay rate of binary pulsar systems
134 can be measured in high precision, which makes pul-
135 sar timing experiments a good tool to test gravitational
136 theories in strong-field regimes (Wex 2014). In previous
137 works, stringent limits have been placed by using recent
138 observational results from binary pulsar systems (Zhao
139 et al. 2019; Shao et al. 2017; Freire et al. 2012; Anto-
140 niadis et al. 2013; Cognard et al. 2017; Anderson et al.
141 2019).

142 There is another class of models, screened modified
143 gravity (SMG), which can evade the tight solar sys-
144 tem constraints by introducing screening mechanisms
145 (Clifton et al. 2012). Various kinds of screen mechanisms
146 have been introduced and studied, such as Chameleon
147 mechanism (Khoury & Weltman 2004a,b), Vainshtein
148 mechanism (Vainshtein 1972; Babichev & Deffayet 2013)
149 and symmetron mechanism (Hinterbichler & Khoury
150 2010). The scalar field can be used to play the role
151 of dark energy for driving the acceleration of the cosmic
152 expansion in cosmological scales. Meanwhile, screening
153 mechanisms can suppress deviations from GR in small
154 scales to circumvent stringent constraints from the solar
155 system tests and laboratorial experiments. (see (Joyce
156 et al. 2015; Clifton et al. 2012; Khoury 2010; Brax 2012)
157 for comprehensive reviews). Numerous tests on SMG
158 have also been performed in different systems (Burrage
159 & Sakstein 2018; Sakstein 2020; Ishak 2018; Zhang et al.

¹ In practice, the possible dependence of G on different circum-
stance is testable in cosmological scale (Zhao et al. 2018).

2019a; Brax et al. 2014; Liu et al. 2018a; Zhang et al. 2019b; Niu et al. 2020; Zhang et al. 2019c).

In recently, the first gravitational wave (GW) event GW150914 was directly detected by LIGO, which confirmed the last remaining not directly detected prediction of GR (Abbott et al. 2016b). And more GW events are captured in the subsequent observing runs by the LIGO-Virgo collaborations (LVC) (Abbott et al. 2019a, 2020c). With the continuing upgrades of sensitivity and the joining of new detectors, GW detections are becoming routines. The GW observations offer a new avenue to test GR and explore the nature of gravity in the extremely strong field regime.

LVC has performed various model-independent tests on observed events, and no evidence for deviations from GR has been found (Abbott et al. 2019a; Collaboration et al. 2020; Abbott et al. 2016a, 2019b). However, for a given specific modified gravity, the model-independent parameters always cannot completely describe the deviations of GWs, which naturally depend on the characters of neutron stars and/or black holes in the corresponding theory. Therefore, it is still interesting to see what constraints on specific models can be given by current observation, which are complementary with the model-independent tests. In this work, we consider three specific scalar-tensor theories mentioned above, BD, DEF and SMG.

Testing scalar-tensor theories by GW has been concerned since the 1990s (Will 1994). Now, more and more detections of GW event and open access data allow us to constrain scalar-tensor theories by real GW data. Since in scalar-tensor gravities, the deviation of GW from that in GR depends on the sensitivity difference of two stars, the asymmetric binaries (e.g. NSBH, white dwarf-NS, white dwarf-BH binaries) are the excellent targets for the model tests.

So far, among all GW events captured by LVC, there are four possible NSBH events, GW200105, GW200115, GW190426_152155 and GW190814 (Abbott et al. 2021a, 2020c,d). The two events, GW200105 and GW200115, released recently, are the first confident observations of NSBH binaries (Abbott et al. 2021a). The component masses of these two events are consistent with current observations of black holes and neutron stars. However, the data are uninformative about the spin or tidal deformation, and no electromagnetic counterparts are detected. There is no direct evidence that the secondaries of these two events are neutron stars. Although it cannot be ruled out that the secondaries are some kind of exotic objects, we follow the most natural interpretation of these two events that they are NSBH coalescence events.

There are also two plausible NSBH events, GW190814 and GW190426_152155 in the second Gravitational-Wave Transient Catalog (GWTC-2). But the nature of these two events is not definitively clear. The secondary mass of GW190814 is about $2.6M_{\odot}$, which could be interpreted as either a low-mass black hole or a heavy neutron star (Abbott et al. 2020d; Most et al. 2020; Broadhurst et al. 2020). However, according to current knowledge and observations of neutron stars, its lighter object is likely too heavy to be a neutron star (Abbott et al. 2020d). We exclude this event in our analysis. Meanwhile, the event GW190426_152155 has the highest false alarm rate (FAR) (Abbott et al. 2020c). Whether it is a real signal of astrophysical origin is still not definitively clear yet. But its component masses are consistent with current understanding of black holes and neutron stars. There are many recent works concerning this event, such as (Broekgaarden et al. 2021; Li et al. 2020; Román-Garza et al. 2020). following some of them, we make our discussion on the assumption that the GW190426_152155 is an NSBH coalescence event. It needs to be emphasized that our analysis will be not applicable if this event is not a real NSBH binary.

There is another obstacle in our analysis. For events with a large mass ratio, deviations have been seen in the posterior distributions of the dipole modification parameter, in which the GR value is excluded from 90% confidence intervals. The case of GW190814 has been shown in the previous works (referring to Appendix C in (Collaboration et al. 2020) and Appendix A in (Perkins et al. 2021) for more detail). We have also seen similar deviations in our analysis of GW200105. The deviations are believed to be unphysical effects which are probably caused by waveform systematics, covariances between parameters, or the way of non-GR modification parameterization. To thoroughly explain these deviations, more studies about the parameterized tests of GR on highly asymmetric sources are needed. In this work, we exclude the event GW200105, and only employ the data of GW200115 and GW190426_152155.

The previous work (Zhao et al. 2019) has used the binary neutron star event in GWTC-1, GW170817, to constrain scalarization effects. However, instead of directly using strain data, They employed the measurement of mass and radius from (Abbott et al. 2018, 2019c) to get the constraints. In this work, we use the modification of dipole radiation in waveform and perform the full Bayesian inference to constrain scalarization effects.

The rest of this paper is organized as follows. In the next section, the modified gravity models considered in this work, including BD, DEF and SMG, are briefly reviewed. Then, in Section 3, we present the basic infor-

mation and principle of data and statistical method used in this work. The results and conclusions are discussed in Section 4. The formulae used to get scalar charges of neutron stars by solving Tolman-Oppenheimer-Volkoff (TOV) equations are presented in Appendix A for convenience of reference. In Appendix B and C, we illustrate the comparisons of posterior distributions of other parameters with the posterior data released by LVC, and compare the constraints on the dipole radiation with the results reported by LVC. We also present the scalar charges gotten from solutions of TOV equations for all four equations-of-state (EoS) considered in this work in Appendix D. A discussion of the other two possible NSBH events which are excluded in the work, GW190814 and GW200105, is presented in Appendix E. All parameter estimation samples of this work are available on Zenodo². Throughout this paper, we use the units in which $\hbar = c = 1$.

2. SCALAR-TENSOR THEORIES

In this work we consider a class of scalar-tensor theories, which can be described by the action

$$S = \frac{1}{16\pi G_*} \int d^4x \sqrt{-g_*} \left[R_* - 2g_*^{\mu\nu} \partial_\mu \varphi \partial_\nu \varphi \right] + S_m \left[\psi_m, A^2(\varphi) g_*^{\mu\nu} \right] \quad (1)$$

in the Einstein-frame. G_* denotes the bare gravitational coupling constant, which is approximated by G when solving TOV equations in practical. $g_*^{\mu\nu}$ and g_* are the Einstein-frame metric and its determinant, and $R_* \equiv g_*^{\mu\nu} R_{\mu\nu}^*$ is the Ricci scalar. The last term is the action of matter, where ψ_m collectively denotes various matter fields and $A(\varphi)$ is the conformal coupling function. Since the potential $V(\varphi)$ will be considered only in the SMG theory, we do not write the $V(\varphi)$ in the above action. The field equations can be derived by varying the action (1) with respect to the metric $g_*^{\mu\nu}$ and scalar field φ ,

$$R_{\mu\nu}^* = 2\partial_\mu \varphi \partial_\nu \varphi + 8\pi G_* \left(T_{\mu\nu}^* - \frac{1}{2} T_*^* g_{\mu\nu}^* \right), \quad (2)$$

$$\square_{g_*} \varphi = -4\pi G_* \alpha(\varphi) T_*,$$

where $\square_{g_*} \equiv (-g_*)^{-1/2} \partial_\mu (\sqrt{-g_*} g_*^{\mu\nu} \partial_\nu)$ is the curved space D'Alembertian, $T_*^{\mu\nu} \equiv 2(-g_*)^{-1/2} \delta S_m / \delta g_{\mu\nu}^*$ is the energy-momentum tensor of matter fields and $T_* \equiv g_{\mu\nu}^* T_*^{\mu\nu}$. The quantity $\alpha(\varphi)$ is defined as $\alpha(\varphi) \equiv \partial \ln A(\varphi) / \partial \varphi$, which describes the coupling strength between the scalar field and matters. The $\ln A(\varphi)$ can be

expanded around the background value φ_0 of the scalar field as

$$\ln A(\varphi) = \alpha_0(\varphi - \varphi_0) + \frac{1}{2} \beta_0(\varphi - \varphi_0)^2 + \mathcal{O}(\varphi - \varphi_0)^3, \quad (3)$$

where the coefficients α_0 and β_0 are related to two parameters β^{PPN} and γ^{PPN} in parameterized post-Newtonian (PPN) formalism by (Will 2018)

$$\gamma^{\text{PPN}} - 1 = -\frac{2\alpha_0^2}{1 + \alpha_0^2}, \quad (4)$$

$$\beta^{\text{PPN}} - 1 = \frac{1}{2} \frac{\alpha_0^2 \beta_0}{(1 + \alpha_0^2)^2}. \quad (5)$$

In the context of compact binary systems, a parameter called the scalar charge, which is defined as

$$\alpha_A \equiv \left. \frac{\partial \ln m_A}{\partial \varphi} \right|_{\varphi=\varphi_0}, \quad (6)$$

can describe the coupling between the scalar field and the star A . This parameter is used to determine the equation of motion and gravitational wave emission of binary systems. For compact binaries in scalar-tensor theories, the center of gravitational binding energy and the center of inertial mass are not coincident, which results in the varying dipole moment and induces extra energy loss by dipole radiation (Will 1994). We consider a gravitational waveform with the leading order of the modification, which has a dipole term in the phase (Will 1994; Tahura & Yagi 2018; Zhang et al. 2017b; Liu et al. 2018b, 2020),

$$h(f) = h_{\text{GR}}(f) \exp \left[i \frac{3}{128\eta} \varphi_{-2} (\pi G M f)^{-7/3} \right], \quad (7)$$

where φ_{-2} is given by

$$\varphi_{-2} = -\frac{5}{168} (\Delta\alpha)^2. \quad (8)$$

The constant coefficients are chosen to keep the same convention of φ_{-2} with LVC's papers (Abbott et al. 2019a; Collaboration et al. 2020; Abbott et al. 2016a, 2019b). $\Delta\alpha \equiv \alpha_A - \alpha_B$ is the difference between scalar charges of two bodies in a binary. For black holes, the no-hair theorem prevents them to acquire scalar charges (Hawking 1972; Bekenstein 1995; Sotiriou & Faraoni 2012; Liu et al. 2018b). In many scalar-tensor theories including the models considered in this work, where the no-hair theorem can be applied, scalar charges of black holes are 0. For neutron stars, scalar charges can be gotten by solving TOV equations.

The detailed process of solving TOV equations to get scalar charges can be found in (Damour & Esposito-Farèse 1993, 1996). We make a brief review in Appendix

² <https://doi.org/10.5281/zenodo.5188445>

334 B for convenience of reference. Inputting the explicit
 335 form of $A(\varphi)$ and $\alpha(\varphi)$, the EoS and the initial condi-
 336 tions to the TOV equations, one can get the physical
 337 quantities α_A , φ_0 and m_A outputted by equations (A4).
 338 The coupling function $A(\varphi)$ and its logarithmic deriva-
 339 tive $\alpha(\varphi)$ are specified by a specific theoretical model,
 340 which will be discussed in the after subsections. For the
 341 EoS, considering the constraints given by the measure-
 342 ment of PSR J0030+0451 (Miller et al. 2019; Riley et al.
 343 2019) and the observation evidence that the maximum
 344 mass of neutron star can be above $2M_\odot$ (Antoniadis
 345 et al. 2013; Cromartie et al. 2019; Demorest et al. 2010;
 346 Fonseca et al. 2016; Arzoumanian et al. 2018), we select
 347 4 widely used EoS, `sly`, `alf2`, `H4` and `mpa1`. The tab-
 348 ulated data of EoS are downloaded from the website³.
 349 To solve the differential equations (A3), the initial con-
 350 ditions,

$$\mu(0) = 0, \nu(0) = 0, \varphi(0) = \varphi_c, \psi(0) = 0, \tilde{p}(0) = p_c, \quad (9)$$

351 need to be passed into the differential equations solver.
 352 In practices, the initial conditions are taken at the place
 353 nearby the center to avoid division by zero. The initial
 354 values of pressure p_c are taken on a dense grid for inter-
 355 polation. The initial condition φ_c is determined by
 356 shooting method. Different φ_c are iteratively tried until
 357 a value which can derive the desired φ_0 is found. In
 358 order to implement Monte Carlo sampling, we need to
 359 get the scalar charge at sufficient speed. It is imprac-
 360 ticable to solve the TOV equations every time when a
 361 likelihood is evaluated. Therefore, we take the values
 362 of model parameters and p_c on a dense grid, and solve
 363 the TOV equations to get the mass and scalar charge
 364 previously. When the Monte Carlo sampler is running,
 365 a set of model parameters and p_c sampled by sampler is
 366 converted to the mass and scalar charge by linear inter-
 367 polation. The interpolation results will be presented in
 368 the after subsections.

369 2.1. Brans-Dicke Theory

370 We firstly consider the Brans-Dicke theory which is
 371 usually seen as the prototype of the scalar-tensor theo-
 372 ries and has been widely studied. The Brans-Dicke theo-
 373 ry is characterized by a linear coupling function given
 374 by

$$A(\varphi) = \exp(-\alpha_0\varphi), \quad (10)$$

375 which lead to a field-independent coupling strength
 376 $\alpha(\varphi) = \alpha_0$. There is another common convention used

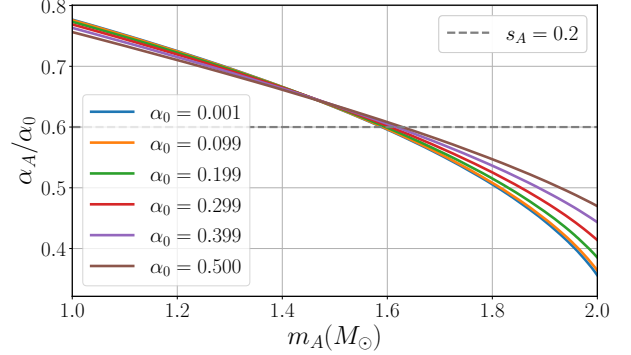


Figure 1. The interpolation result $\alpha_A(\alpha_0, m_A)$ of EoS `sly`. The gray dashed horizontal line denotes the sensitivity $s_A = 0.2$ which is a approximation commonly used in literature.

377 in literature (Will 2014),

$$\alpha_0^2 = \frac{1}{3 + 2\omega_{\text{BD}}}. \quad (11)$$

378 Given the specific form of coupling function (10), we
 379 can use the process discussed in the last subsection to
 380 get the scalar charge of a neutron star. Inputting an
 381 initial condition (9) and an EoS, we can get the numer-
 382 ical solutions of a neutron star structure by integrating
 383 the TOV equations (A3). And the quantities, α_A , φ_0
 384 and m_A can be extracted from the solutions by (A4).
 385 The initial condition p_c and the model parameter α_0
 386 are taken on a dense grid for facilitating the interpola-
 387 tion. The last degree of freedom is the asymptotic scalar
 388 field φ_0 which is set to 0 and the initial condition φ_c is
 389 gotten by the shooting method. In order to reduce the
 390 computational burden, we use an interpolated relation
 391 $\alpha_A(\alpha_0, m_A)$ in the Monte Carlo sampling. We present
 392 the interpolation result of EoS `sly` as an example in Fig-
 393 ure 1, and results for other EoS can be seen in Appendix
 394 D.

395 Another parameter which called sensitivity, s_A , is also
 396 commonly seen in literature. The sensitivity and the
 397 scalar charge are related by (Palenzuela et al. 2014;
 398 Sampson et al. 2014)

$$\alpha_A = \frac{1 - 2s_A}{\sqrt{3 + 2\omega_{\text{BD}}}}. \quad (12)$$

399 Some works, such as (Zhang et al. 2017b), employ $s_A =$
 400 0.2 as a convenient approximation. We illustrate this
 401 approximation in Figure 1 by the gray dashed horizontal
 402 line for comparing with the results gotten by solving
 403 TOV equations.

404 2.2. Theory with Scalarization Phenomena

³ http://xtreme.as.arizona.edu/NeutronStars/data/eos_tables.tar

In the Brans-Dicke theory, all possible deviations from GR are in the order of α_0^2 in both weak-field regimes and strong-field regimes (Will 2018; Damour & Esposito-Farèse 1993). More generally, in generic scalar-tensor theories, all possible deviations from GR can be expanded as a series of powers of α_0^2 , which has the schematic form as (Esposito-Farèse 2004; Damour & Esposito-Farèse 1992)

$$\text{deviation} \sim \alpha_0^2 \times \left[\lambda_0 + \lambda_1 \frac{Gm}{R} + \lambda_2 \left(\frac{Gm}{R} \right)^2 + \dots \right], \quad (13)$$

where m and R are mass and radius of a star, $\lambda_0, \lambda_2, \dots$ are constant coefficients constructed from α_0, β_0, \dots in the expansion (3). Since the solar system experiments have placed very stringent constraints on α_0 , it is plausible that all possible deviations from GR in other experiments are expected to be small. The work of Damour and Esposito-Farèse (Damour & Esposito-Farèse 1993) shown that such opinions are illegitimate. In the strong-field regime, when the compactness Gm/R exceeds a critical value, some nonperturbative effects can emerge, the part of square brackets in expansion (13) can compensate the small α_0^2 , order-of-unit deviations from GR can still be developed.

Following the model discussed by Damour and Esposito-Farèse in (Damour & Esposito-Farèse 1993), we consider the coupling function with a quadratic term,

$$\ln A(\varphi) = \frac{1}{2} \beta_0 \varphi^2. \quad (14)$$

The corresponding α_0 is given by

$$\alpha_0 = -\alpha(\varphi_0) = -\beta_0 \varphi_0. \quad (15)$$

It has been shown in (Damour & Esposito-Farèse 1993), when $\beta_0 < 0$, the local value of $\alpha(\varphi)$ can be amplified with respect to its asymptotic value α_0 . The nonperturbative amplification effects are expected to take place when $\beta_0 \lesssim -4$. These nonperturbative amplification effects named spontaneous scalarization can lead to a phase transition in a certain range of mass. While, if the β_0 is positive, the deviations from GR are further quenched. In this work, we only consider the negative branch. It returns to GR when $\alpha_0 = \beta_0 = 0$.

The scalar charge of a neutron star can be gotten by solving TOV equations as discussed before. We present the result of the EoS `sly` in Figure 2 as an example. There are two parameters ($\log_{10} \alpha_0, \beta_0$) characterizing the model in this case. We use colors to denote different values of β_0 , and line styles for $\log_{10} \alpha_0$. The parameter α_0 is related to the weak-field effects. We consider the range of α_0 under the priori constraint of

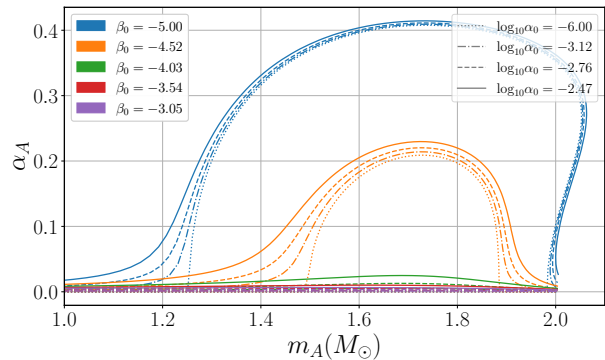


Figure 2. Nonperturbative strong-field effects in DEF. The results of one EoS `sly` are shown as an example. Different colors are used to denote different values of β_0 and line styles for $\log_{10} \alpha_0$. When $\beta_0 < -4$, the nonperturbative strong-field effects emerge, which leads to a phase transition in a certain range of mass and allows the scalar charge to be large even if the α_0 is vanishingly small. The nonzero α_0 can smooth the phase transition. The varying of the scalar charge as a function of the mass is smoother for larger α_0 .

Cassini $\alpha_0 < 3.4 \times 10^{-3}$ (Shao et al. 2017; Bertotti et al. 2003; Damour 2007). Besides, the larger α_0 can smooth the phase transition when scalarization phenomena occur (Damour & Esposito-Farèse 1996). For β_0 , it is the parameter that can control whether the spontaneous scalarization could happen in strong-field regimes. As can be seen in Figure 2, when $\beta_0 < -4$, the scalar charge can be large even if the α_0 is vanishingly small for a certain range of mass. The mass ranges where the spontaneous scalarization can occur are different for different EoS (Shao et al. 2017; Shibata et al. 2014). Therefore, unlike BD, the relations between the scalar charge and the mass of DEF have obvious differences for different EoS. More details will be presented in Appendix D.

The results gotten by solving TOV equations are interpolated for stochastic sampling. Due to the scalarization phenomena, the curves representing the scalar charge as functions of the mass have the intricate behavior of hysteresis phenomena. In order to facilitating the interpolation, instead of the mass, we use the initial condition of pressure p_c as the parameter sampled in Monte Carlo sampling and generate the interpolation function of $\alpha_A(\log_{10} \alpha_0, \beta_0, p_c)$ and $m_A(\log_{10} \alpha_0, \beta_0, p_c)$. The results of one EoS `sly` are shown in Figure 3.

2.3. Screened Modified Gravity

The third model we considered is screened modified gravity (SMG). Besides the coupling function $A(\varphi)$ characterizing the interaction between the scalar field and the matter field, there is the potential $V(\varphi)$ character-

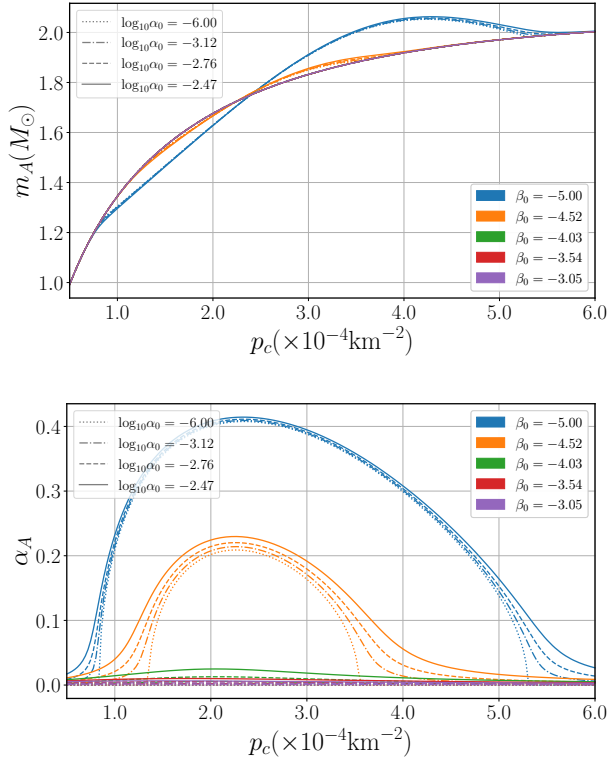


Figure 3. Interpolation results of $m_A(\log_{10} \alpha_0, \beta_0, p_c)$ and $\alpha_A(\log_{10} \alpha_0, \beta_0, p_c)$ used in stochastic sampling. We present the results of one EoS `sly` as an example. Since the relations between the scalar charge and the mass have the hysteresis phenomena, which brings difficulties to interpolation, we use the parameter p_c instead of the mass in the stochastic sampling. The parameters $(\log_{10} \alpha_0, \beta_0, p_c)$ are converted to the parameters (α_A, m_A) which are needed to generate a waveform by the interpolation of $m_A(\log_{10} \alpha_0, \beta_0, p_c)$ and $\alpha_A(\log_{10} \alpha_0, \beta_0, p_c)$ shown in this figure.

izing the self-interaction of the scalar field. The coupling function $A(\varphi)$ and the potential $V(\varphi)$ define the effective potential $V_{\text{eff}}(\varphi)$ which controls the behavior of the scalar field. The scalar field acquires the mass around the minimum of the effective potential $V_{\text{eff}}(\varphi)$, which depends on the environmental density. The mass of the scalar field can be large in high density regions and the range of the fifth force becomes short, so the effects of the scalar field are screened. While, on large scales, the environmental density is low, the scalar field becomes light and can affect the galactic dynamic or the universe expansion acceleration. (See comprehensive review (Ishak 2018) for more different types of screening mechanism.) For the general SMG with canonical ki-

netic energy term, we can rewrite the action as

$$S = \int d^4x \sqrt{-g_*} \left[\frac{1}{16\pi G} R_* - \frac{1}{2} g_*^{\mu\nu} \partial_\mu \varphi \partial_\nu \varphi - V(\varphi) \right] + S_m \left[\psi_m, A^2(\varphi) g_*^{\mu\nu} \right], \quad (16)$$

where bare potential $V(\varphi)$ characterizes the scalar self-interaction, which endows the scalar field with mass. There are many SMG models in the market, including the chameleon, symmetron, dilaton and $f(R)$ models, in which the functions $V(\varphi)$ and $A(\varphi)$ are chosen as the specific forms (Zhang et al. 2016; Liu et al. 2018a). The scalar field equation of motion can be yielded by varying the action with respect to φ ,

$$\square_{g_*} \varphi = \frac{\partial}{\partial \varphi} V_{\text{eff}}(\varphi), \quad (17)$$

where the effective potential is defined as

$$V_{\text{eff}}(\varphi) = V(\varphi) - T_*. \quad (18)$$

The waveform of gravitational waves from inspiraling compact binaries in SMG has been given in the previous work (Liu et al. 2018b). As mentioned above, we only consider the leading order modification which is the dipole term shown in equations (7) and (8). Since the effects of the scalar field are suppressed due to the screening mechanism, the scalar charges of neutron stars are expected to be small. Therefore, we do not solve the TOV equations to get the scalar charge, but adopt a simple approximation that considers a neutron star as a static spherical symmetric object with constant density. The scalar field equation (17) can be simplified and solved directly to get the exact solution. Matching the internal and external solutions, the scalar charge of a neutron star in SMG can be given by (see Appendix A in (Zhang et al. 2017a) for more details)

$$\alpha_A = \frac{\varphi_{\text{VEV}}}{M_{\text{Pl}} \Phi_A}, \quad (19)$$

where $M_{\text{Pl}} = \sqrt{1/8\pi G}$ is the reduced Planck mass, φ_{VEV} is the vacuum expectation value of the scalar field, and $\Phi_A = Gm/R$ is the surface gravitational potential of the object A .

3. PUBLIC DATA AND BAYESIAN METHOD

3.1. Public Gravitational Wave Data

Among all GW events released by LVC, there are four possible NSBH events (Abbott et al. 2021a, 2020c,d), GW190426_152155, GW190814, GW200105, GW200115, and two (possible) binary neutron star (BNS) events (Abbott et al. 2017a, 2020a), GW170817,

GW190425, which could potentially be used for the tests on scalar-tensor theories.

For convenience of reference, we list some basic information of these 6 events in Table 1 and present a brief review of these events below. GW170817 (Abbott et al. 2017a) is a relatively confident BNS event since its electromagnetic counterpart was captured by various facilities across the electromagnetic spectrum (Abbott et al. 2017b). While definite electromagnetic counterpart observations for the all other events are absent. For GW190425 (Abbott et al. 2020a), the mass of its components is consistent with neutron stars, but its total mass and chirp mass are larger than those of any other known binary neutron star systems. It cannot be ruled out by GW data alone that one or both of its components are black holes. GW190814 (Abbott et al. 2020d) is a stranger event with its significantly unequal mass ratio and unusual secondary component. It involves a $22.2\text{--}24.3M_{\odot}$ black hole and a $2.50\text{--}2.67M_{\odot}$ object which we do not know much about yet. All current models of formation and mass distribution for compact binaries are challenged by this event. GW190426_152155 (Abbott et al. 2020c) is a possible NSBH event, since the mass of its components is consistent with our current understanding of neutron stars and black holes. But this event has the highest false alarm rate (FAR), 1.4yr^{-1} , which obscures that whether it is a real signal of astrophysical origin. Besides, since the data are uninformative about the effects such as tidal deformability or spin-induced quadrupole, it also cannot be ruled out that its secondary object is a black hole or other exotic objects. GW200105 and GW200115 are two NSBH coalescence events reported recently (Abbott et al. 2021a). The primaries and secondaries of these two binaries have the masses within the range of known black holes and neutron stars respectively. These two events have been regarded as the first observations of NSBH binaries via any observational means. Note that, although the most natural interpretations of these two events are NSBH coalescences, this conclusion is inferred only by their component masses. Until now, there is no direct evidence, such as tidal or spin deformation and electromagnetic counterparts. It is still difficult to rule out that the secondaries are other objects.

Although there are 6 events that probably include at least one neutron star in the current GW catalog, only two events, GW190426_152155 and GW200115, can be used in this work.

For GW190814, due to its unusual mass ratio which is in a region that has not been systematically studied, the issue of waveform systematics can lead to some kind of unphysical deviation (referring to Appendix C

in (Abbott et al. 2020c) and Appendix A in (Perkins et al. 2021) for more details). And within our knowledge, there are no EoS can reach the mass of its secondary object and meanwhile be favored by current observations of neutron stars. We exclude this event in our discussion.

One of two NSBH events reported recently, GW200105, also has a large mass ratio, which can be seen in Figure 14. The similar unphysical deviation is also present in the analysis of this event. We show the posterior distribution of the dipole modification parameter in Figure 13. The GR value falls in the tail of the posterior and is excluded from the 90% confidence interval. This deviation is believed to be unphysical, which might be the consequences of systematic errors of waveform templates, covariances between parameters, or the way of the parametrization of non-GR modification (Abbott et al. 2020c; Perkins et al. 2021). We present more discussion on this issue in Appendix E, and exclude this event in the main body of this work.

For GW170817 and GW190425, only one side limit on the mass ratio can be placed, which means the situation that the two components have an equal mass cannot be ruled out. The dipole radiation depends on the difference of the scalar charges between two components of a binary. As shown in Figures 1 and 2, the scalar charges are functions of mass for BD $\alpha_A(\alpha_0, m)$ and DEF $\alpha_A(\alpha_0, \beta_0, m)$. The symmetrical binaries can lead to very long tails in posterior distributions of α_0 or (α_0, β_0) which cannot descend to zero when reaching the boundary of whatever prior setting. Therefore, even the two BNS events can place very strong bounds on the dipole amplitude, we cannot use them to place any effective constraints on model parameters of BD or DEF. But we can constrain the dipole radiation for GW170817 and GW190425 without considering specific model parameters. In order to compare with the results from LVC, we also perform the constraints on φ_{-2} for these two events in Appendix C.

Although the origin of GW190426_152155 still has some uncertainty, the data are consistent with a GW signal from NSBH coalescence. We think it is feasible to test modified gravity models using this event. The results can at least offer a reference for future more confident NSBH events.

As discussed above, the events GW190426_152155 and GW200115 are the only two left that can be used for our purpose. The data are downloaded from Gravitational Wave Open Science Center⁴ (Abbott et al. 2021b) and down-sampled to 2048Hz. Besides strain data, power

⁴ <https://doi.org/10.7935/99gf-ax93>

spectral densities (PSDs) are also needed for parameter estimation (Abbott et al. 2020b). Instead of directly estimating PSDs from strain data by the Welch method, we use the event-specific PSDs which are encapsulated in LVC posterior sample releases for specific events (LVC 2020a; LIGO Scientific Collaboration and Virgo Collaboration 2020). These PSDs are expected to lead to more stable and reliable parameter estimation (Abbott et al. 2019a; Cornish & Littenberg 2015; Littenberg & Cornish 2015). As mentioned above, we only consider inspiral stages, therefore the frequency corresponding to the innermost stable circular orbit (ISCO),

$$f_{\text{ISCO}} = \frac{1}{6^{3/2}\pi M}, \quad (20)$$

where M denotes the total mass of the binary, is chosen as the maximum frequency cutoff (Buonanno et al. 2009). The minimum frequency cutoffs are chosen by following LVC’s papers (Abbott et al. 2020c, 2021a). The frequency of GW from inspiral of compact binary in circular orbit evolves with time. The data segment durations are set to be consistent with this frequency range. The data segment is positioned such that there are two seconds post-trigger duration (Romero-Shaw et al. 2020).

3.2. Bayesian Method

Bayesian inference is broadly used in modern science for extracting useful information from noisy data. Bayesian inference allows us to make statements on how probabilities of parameters distribute in priori ranges based on the observed data in a specific model. In the context of GW astronomy, given a model M described by a set of parameters θ , observed strain data \mathbf{d} , and background information I which determines the likelihood and prior, the Bayes’ theorem can be written as (Abbott et al. 2020b; Bayes 1763)

$$p(\theta|\mathbf{d}, M, I) = p(\theta|M, I) \frac{p(\mathbf{d}|\theta, M, I)}{p(\mathbf{d}|M, I)}. \quad (21)$$

The left-hand side is the posterior probability density function of model parameters, which is the product of Bayesian inference and represent the result inferred from data. The three terms on right-hand denote the prior probability density $p(\theta|M, I)$, the likelihood $p(\mathbf{d}|\theta, M, I)$, and the evidence $p(\mathbf{d}|M, I)$. Under the assumption that the noise from detectors is stationary and Gaussian, the likelihood function can be written as (Cutler & Flanagan 1994; Romano & Cornish 2017)

$$p(\mathbf{d}|\theta, M, I) \propto \exp \left[-\frac{1}{2} \sum_i \langle \mathbf{h}(\theta) - \mathbf{d} | \mathbf{h}(\theta) - \mathbf{d} \rangle \right], \quad (22)$$

where i denotes different detectors, $\mathbf{h}(\theta)$ is the waveform template. The angle brackets represent the noise-weighted inner product defined as

$$\langle \mathbf{a} | \mathbf{b} \rangle = 4\Re \int \frac{a(f)b^*(f)}{S_n(f)} df \quad (23)$$

with the noise power spectral density (PSD) $S_n(f)$ of the detector.

As discussed in Section 2, we consider a waveform model including a term of dipole radiation. The waveform template used to compute likelihood is obtained by slightly modifying the aligned-spin with tidal deformability waveform IMRPhenomD_{NRTidal} (Dietrich et al. 2019) which have been implemented in the LIGO Algorithm Library LALSuite (LIGO Scientific Collaboration 2018).

For the prior, a range needs to be set for each parameter of the model. As discussed above, instead of the mass parameter, we choose the central pressure of neutron star as a model parameter. The prior ranges are set by referring to (Romero-Shaw et al. 2020; Abbott et al. 2019a). According to the known properties of binary neutron stars, we employ the low-spin prior in this work (Abbott et al. 2019c; Stovall et al. 2018; Burgay et al. 2003). The evidence plays the role of the normalization factor and is also used in model selection.

One of the obstacles to applying Bayesian inference is the extremely costly computation. For the huge parameter space, it is impractical to evaluate the likelihood on a grid. The Markov chain Monte Carlo (MCMC) methods (Metropolis et al. 1953; Hastings 1970) or nested sampling methods (Skilling 2006, 2004) are commonly used to estimate the posterior distribution by sampling in parameter space. We use the open-source library Bilby⁵ (Ashton et al. 2019) with the nested sampler Dynesty⁶ (Speagle 2020) to do our Bayesian inference. The sampler settings are chosen by referring to (Romero-Shaw et al. 2020).

4. RESULTS AND CONCLUSIONS

We will present our results in this section. All our results are consistent with GR. For the parameter β_0 in DEF, we find the constraints given by GWs are comparable with the previous constraints given by pulsar timing experiments. For BD and SMG, the constraints are not competitive with the current bounds placed by the solar system experiments. We do not find significant differences among the constraints using different EoS. More details are in the following.

⁵ <https://github.com/lscsoft/bilby>

⁶ <https://github.com/joshspeagle/dynesty>

event	type	$m_1(M_\odot)$	$m_2(M_\odot)$	SNR	FAR(yr^{-1})
GW170817	BNS	$1.46^{+0.12}_{-0.10}$	$1.27^{+0.09}_{-0.09}$	33.0	$\leq 1.0 \times 10^{-7}$
GW190425	BNS(?)	$2.0^{+0.6}_{-0.3}$	$1.4^{+0.3}_{-0.3}$	13.0	7.5×10^{-4}
GW190426_152155*	NSBH(?)	$5.7^{+3.9}_{-2.3}$	$1.5^{+0.8}_{-0.5}$	10.1	1.44
GW190814	NSBH(?)	$23.2^{+1.1}_{-1.0}$	$2.6^{+0.08}_{-0.09}$	22.2	$\leq 1.0 \times 10^{-5}$
GW200105	NSBH	$8.9^{+1.2}_{-1.5}$	$1.9^{+0.3}_{-0.2}$	13.9	0.36
GW200115*	NSBH	$5.7^{+1.8}_{-2.1}$	$1.5^{+0.7}_{-0.3}$	11.6	$\leq 1.0 \times 10^{-5}$

Table 1. Some basic information on 6 events which probably include at least one neutron star are listed for convenience of reference. The data are copied from Gravitational Wave Open Science Center (www.gw-openscience.org). The two events with stars are used to place the constraints in this work.

4.1. Brans-Dicke Theory

For BD, the posterior distributions of α_0 are shown in Figure 4. The posteriors of two events can be combined together (Agathos et al. 2014; Abbott et al. 2019d), and the combined results are shown by the gray lines with translucent shading. The vertical dashed lines denote the upper limits of α_0 at 90% confidence level (CL) whose exact values are collected in Table 2. Colors are used to denote two events. In the results, the impact of difference EoS is invisible within statistical errors. According to the relation (11), one can get the constraints on ω_{BD} which are also shown in Table 2. So far, the most stringent constraint on BD is from the measurement of Shapiro time delay performed Cassini spacecraft which places the bound (Bertotti et al. 2003),

$$\gamma^{\text{PPN}} - 1 = (2.1 \pm 2.3) \times 10^{-5}. \quad (24)$$

The corresponding constraint on ω_{BD} is (Will 2014)

$$\omega_{\text{BD}} > 40000. \quad (25)$$

The pulsar timing experiments also place the constraint (Freire et al. 2012; Antoniadis et al. 2013; Zhang et al. 2019a)

$$\omega_{\text{BD}} > 13000. \quad (26)$$

We summarize the different constraints in the Table 3 for comparison. The constraints given by GWs have no competition with these current constraints. This result is expectable. In Zhang et al. (2017b), we found that in the third-generation GW detector era, the bound by combining a larger number of GW events is expected to be better than that derived in Solar system.

4.2. Theory with Scalarization Phenomena

For DEF, we plot the posterior distributions of $(\log_{10} \alpha_0, \beta_0)$ in Figure 5 and summarize the combined constraints of parameter β_0 in Table 2. In Figure 5, we show the 90% CL regions of the joint posterior distributions for $(\log_{10} \alpha_0, \beta_0)$ in the main panels, and the marginalized posteriors for $\log_{10} \alpha_0$ and β_0 are plotted

	BD		DEF
	α_0	ω_{BD}	β_0
sly	$\lesssim 0.123$	$\gtrsim 31.5$	$\gtrsim -3.93$
alf2	$\lesssim 0.109$	$\gtrsim 40.6$	$\gtrsim -4.00$
H4	$\lesssim 0.103$	$\gtrsim 45.6$	$\gtrsim -3.77$
mpa1	$\lesssim 0.114$	$\gtrsim 37.0$	$\gtrsim -4.08$

Table 2. The values of 90% CL limits of combined posteriors for the model parameter in BD, α_0 , and its corresponding ω_{BD} , as well as the parameter β_0 in DEF.

in the side panels. The blue and orange lines denote the two events respectively and gray lines with translucent shading denote the combined results.

Although the mass ranges where the scalarization can occur are different for different EoS (Shao et al. 2017; Shibata et al. 2014), we do not find the results have obvious differences beyond statistical errors for different EoS. It returns to GR when $\alpha_0 = \beta_0 = 0$. Our results are consistent with GR and have no evidence for scalarization phenomena. There are some features in Figure 5 which might be noteworthy.

The posterior distributions of β_0 are almost flat when $\beta_0 > -4$. This is because the scalarization phenomena cannot occur in this range. As can be seen in Figure 2 and the bottom panel of Figure 3, in the range of $\beta_0 > -4$, the nonperturbative effects will not take place for any neutron star mass. The scalar charges are almost independent of β_0 . Different values of β_0 can hardly be distinguished by the sampling algorithm. Hence, the posterior distributions are flat in this range.

The posteriors of $\log_{10} \alpha_0$ distributes uniformly on the prior range, which shows no difference with the prior distribution. The two-dimensional joint distribution in the main panel of Figure 2 also shows that the different values of $\log_{10} \alpha_0$ are totally indistinguishable for the stochastic sampler. On the one hand, in the range of $\beta_0 > -4$ where the nonperturbative amplification effects cannot occur, it returns to the case like the Brans-Dicke

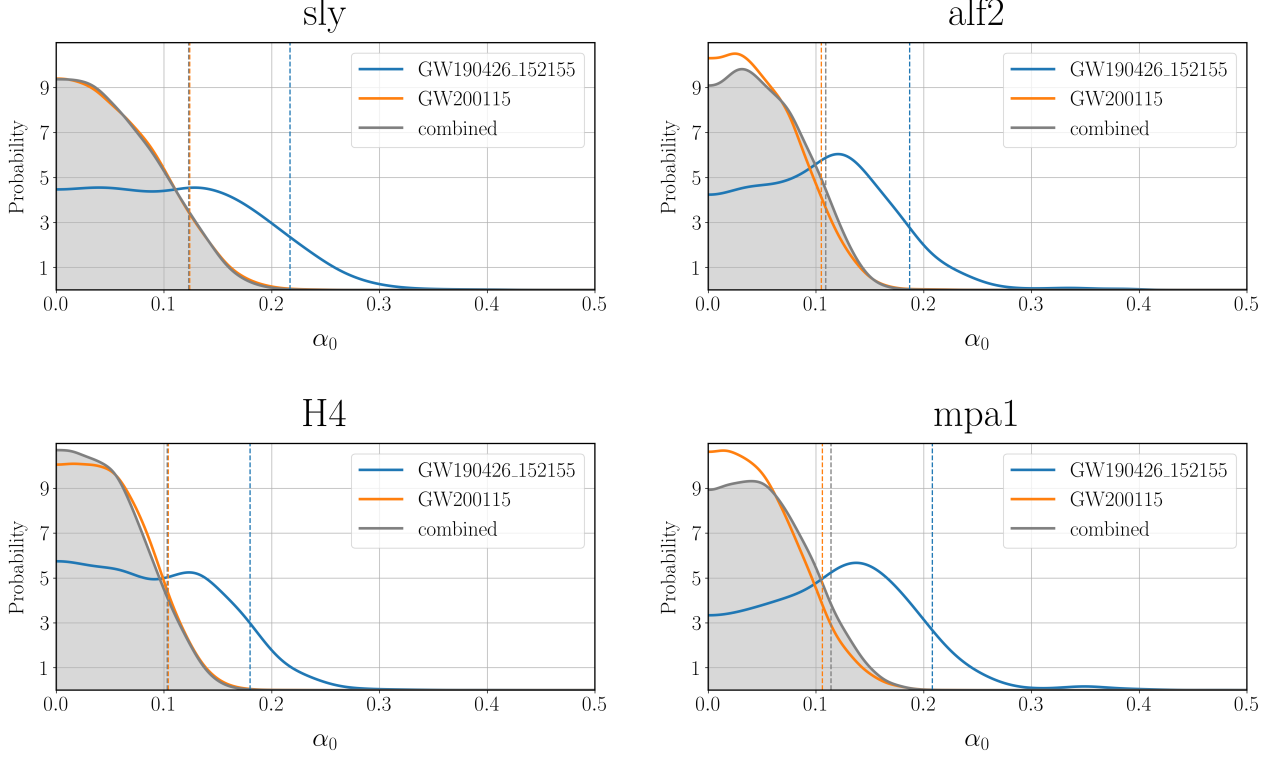


Figure 4. Posterior distributions of α_0 for BD. The results of two events are shown by blue and orange lines. The gray lines with translucent shading denote the combined posterior distributions. The dashed vertical lines indicate the upper limits at 90% CL.

778 theory. And we adopt the prior range compatible with
 779 the Cassini constraint, in which the values of α_0 are
 780 vanishingly small. Any scalar charges evaluated in this
 781 region are too small to cause detectable effects. Different
 782 values of β_0 and $\log_{10} \alpha_0$ cannot be distinguished by
 783 the sampler in this region. On the other hand, even
 784 in the range of $\beta_0 < -4$, as can be seen in Figure 2
 785 and 3, the influence on the scalar charges of $\log_{10} \alpha_0$ is
 786 much smaller than β_0 . The small difference caused by
 787 $\log_{10} \alpha_0$ cannot be detected by the noisy GW data. Due
 788 to these reasons, we cannot place the constraints on the
 789 parameter $\log_{10} \alpha_0$ from our sampling results.

790 It is useful to compare our results with the previous
 791 similar works (Shao et al. 2017; Zhao et al. 2019), which
 792 used pulsar timing experiments to constrain DEF. In the
 793 work (Zhao et al. 2019), GW event GW170817 are also
 794 considered to place the constraints. Different from the
 795 full Bayesian method in which the waveform templates
 796 and the power spectral density are used to construct
 797 the likelihood function, they employed the measurement
 798 results of mass and radii to construct the likelihood.
 799 Another difference is that we use the prior range of $-6 <$
 800 $\beta_0 < 0$ which can return to GR at the edge. While, in
 801 the works (Shao et al. 2017; Zhao et al. 2019), they are
 802 only interested in the range $\beta_0 \in [-5, -4]$ where the

803 scalarization can take place. They present the 90% CL
 804 bounds

$$\beta_0 \gtrsim -4.3. \quad (27)$$

805 Our constraints of β_0 are better in the order of 0.3.
 806 However, considering the statistical errors, we think this
 807 difference is not significant. The different prior setting
 808 may also induce this slight difference. For α_0 , they can
 809 place the constraint $\alpha_0 \lesssim 10^{-4}$. While the different val-
 810 ues of $\log_{10} \alpha_0$ are indistinguishable in our sampling. As
 811 discussed above, due to the statistical uncertainty and
 812 the reason that we consider the prior of β_0 including the
 813 range where the scalarization cannot occur, we cannot
 814 constrain $\log_{10} \alpha_0$. As can be seen in Figure 15 of Ap-
 815 pendix A in the work (Zhao et al. 2019), The parameter
 816 $\log_{10} \alpha_0$ also cannot be constrained well by using the
 817 GW only. The constraints given by GW170817 in the
 818 work (Zhao et al. 2019) are a little more related to EoS
 819 comparing to our results. This is because of the different
 820 mass parameters of two GW events. The primary and
 821 secondary mass of GW170817 with the low-spin prior
 822 assumption at 90% CL are given by (Abbott et al. 2018,
 823 2019c) $m_1 \in (1.36, 1.60)$ and $m_2 \in (1.16, 1.36)$. As can
 824 be seen in Figure 12, the scalarization phenomena on
 825 these ranges depend on the EoS more strongly. While,

the secondary masses of the two events considered here are heavier and in the range where the dependence of scalarization phenomena on EoS is less. We summarize the comparisons in Table 3

4.3. Screened Modified Gravity

The third model we discussed is SMG. As mentioned in Section 2, the screening mechanism can suppress the effects of the scalar field in high density regions. The scalar charges of neutron stars are expected to be small. Hence, for SMG we do not consider different EoS and strictly solve the TOV equations but adopt a simple approximation which considers neutron stars have a constant density to get the scalar charges as presented in the equation (19). We use the typical value $m = 1.4M_\odot$ and $R = 10\text{km}$ for the surface gravitational potential Φ_A in the equation (19). Since this scalar charge is independent with other parameters under the approximation, we do not sample parameters of specific SMG models. Whereas, we sample the parameter φ_{-2} in the equation (7) and place the constraint on φ_{VEV} by the upper limit of φ_{-2} . Constraining the parameter φ_{-2} is similar with the model-independent parameterized tests of GW generation performed by LVC (Abbott et al. 2019a; Collaboration et al. 2020; Abbott et al. 2019b), except for two differences. Since we are discussing the specific model, it is more logical to take physical limits into consideration. For the models considered in this works, the dipole radiations always take energy away and the outgoing energy flux is positive. The phase evolution will be ahead comparing with the case of GR. So, we consider the prior range constraining $\varphi_{-2} \leq 0$. Another difference is that we only consider the inspiral range. Since we are ignorant about the waveform in the merge and ringdown range for scalar-tensor theories, we adopt the cutoff at the frequency corresponding to ISCO as shown in the equation (20).

The posterior distribution of φ_{-2} is shown in Figure 6. The combined constraint at 90% CL is

$$\varphi_{-2} > -2.2 \times 10^{-4}, \quad (28)$$

and the corresponding constraint on φ_{VEV} is given by

$$\frac{\varphi_{\text{VEV}}}{M_{\text{Pl}}} < 1.8 \times 10^{-2}. \quad (29)$$

The constraint on φ_{-2} by GW170817 is about 10^{-5} (Abbott et al. 2019b) which is one order magnitude better than the constraint given here. This better constraint is because that there are more circles that can be monitored for GW170817. Since GW170817 is lighter than the two events considered here, in the detectors sensitive band the signal can be observed is longer and the circles

can be tracked is more. We show the posterior distributions of φ_{-2} given by GW170817 and another possible binary neutron star event GW190425 in Appendix C for convenience of comparison.

The parameter φ_{VEV} has also be constrained by the solar system tests and pulsar timing experiments. The most stringent constraint in the solar system is from lunar laser ranging (LLR) measurement (Hofmann et al. 2010; Zhang et al. 2019a), which is given by

$$\frac{\varphi_{\text{VEV}}}{M_{\text{Pl}}} < 7.8 \times 10^{-15}. \quad (30)$$

Pulsar timing experiments also place the constraint (Freire et al. 2012; Antoniadis et al. 2013; Zhang et al. 2019a)

$$\frac{\varphi_{\text{VEV}}}{M_{\text{Pl}}} < 4.4 \times 10^{-8}. \quad (31)$$

These constraints are much better than the constraint gotten in this work. On one hand, these much stronger constraints are caused by the fact that the surface gravitational potentials of white dwarfs and objects in the solar system are much less than those in neutron stars. The difference of compact between white dwarfs and neutron stars can be about $\Phi_{\text{WD}}/\Phi_{\text{NS}} \sim 10^{-4}$. This ratio will be much less for objects in the solar system. On the other hand, after the GW signal enters the sensitive band, there are only tens of seconds left before the final plunge in. Whereas the pulsar timing experiments can monitor the orbital motion of a binary at lower frequency and in longer time. And the experiments in the solar system can also collect data over long time.

5. SUMMARY

As more and more various kinds of GW events are observed, GW is becoming an important tool to test GR and explore the nature of gravity. The open access data and user-friendly software tools engage the community to take part in the research about gravitational waves more broadly. Although various model-independent tests have been performed by LVC and placed stringent upper limits on possible deviations from GR, it is still interesting to ask what constraints on specific models can be placed by last observations. In this work, we consider three specific scalar-tensor theories, the Brans-Dicke theory (BD), the theory with scalarization phenomena proposed by Damour and Esposito-Farèse (DEF) and the screened modified gravity (SMG).

The data used in this work are the possible NSBH coalescence GW event GW190426_152155 in GWTC-2 and one of the two confident NSBH events reported recently GW200115. Due to the possible unphysical deviations, we exclude the events GW190814 and GW200105 in this

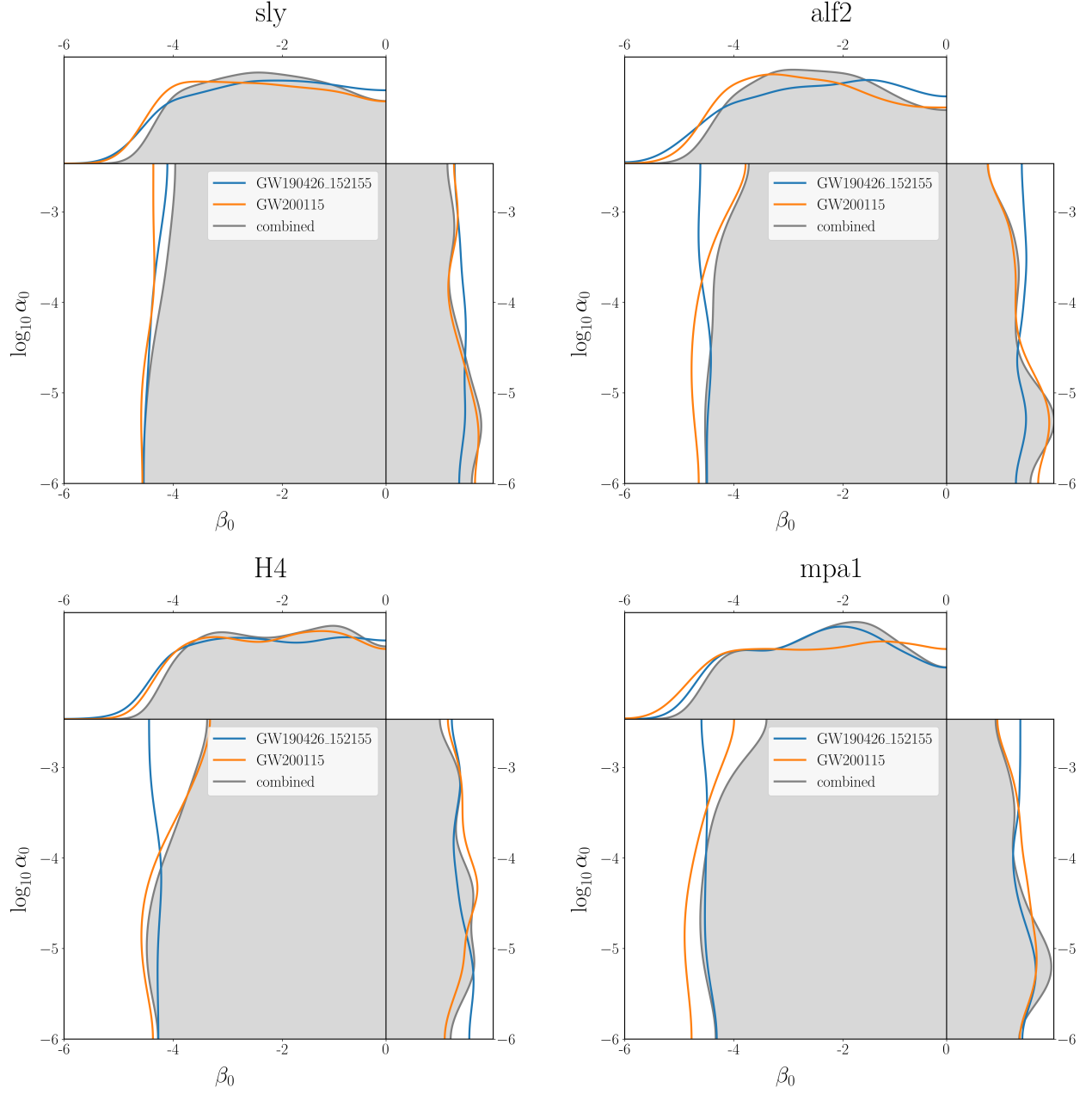


Figure 5. The posterior distributions of parameters $(\log_{10} \alpha_0, \beta_0)$ in DEF. The 90% CL regions of the joint posterior distributions for $(\log_{10} \alpha_0, \beta_0)$ are shown in the main panels, and the marginalized posteriors for $\log_{10} \alpha_0$ and β_0 are plotted in the side panels. The posterior distributions of two events are indicated by two different colors and the combined posteriors are shown by the gray lines with translucent shading. It returns to GR when $\alpha_0 = \beta_0 = 0$. The results show consistency with GR and no evidence for scalarization phenomena. In the range of $\beta > -4$, the scalarization cannot occur and the scalar charges are almost zero. The different values of β_0 can hardly be distinguished. Therefore, the distributions of β_0 are flat in this range. Since we require the prior of $\log_{10} \alpha_0$ to be compatible with the Cassini constraint and the influence on the scalar charges of $\log_{10} \alpha_0$ is too small to be detected, the different values of $\log_{10} \alpha_0$ in its prior range are totally indistinguishable by the stochastic sampler.

	solar system	pulsar timing	GWs(combined)	GWs(only GW200115)
BD	$\omega_{\text{BD}} \gtrsim 40000$	$\omega_{\text{BD}} \gtrsim 13000$	$\omega_{\text{BD}} \gtrsim 40$	$\omega_{\text{BD}} \gtrsim 40$
DEF	-	$\beta_0 \gtrsim -4.3$	$\beta_0 \gtrsim -4.0$	$\beta_0 \gtrsim -4.2$
SMG	$\frac{\varphi_{\text{VEV}}}{M_{\text{Pl}}} \lesssim 7.8 \times 10^{-15}$	$\frac{\varphi_{\text{VEV}}}{M_{\text{Pl}}} \lesssim 4.4 \times 10^{-8}$	$\frac{\varphi_{\text{VEV}}}{M_{\text{Pl}}} \lesssim 1.8 \times 10^{-2}$	$\frac{\varphi_{\text{VEV}}}{M_{\text{Pl}}} \lesssim 1.8 \times 10^{-2}$

Table 3. Different constraints are summarized for convenience of comparison. We also list the results that are given by the events GW200115 only, in case the event GW190426_152155 is believed to be a false GW signal. However, for BD and SMG, differences between the combined results and the results excluding GW190426_152155 are within the round-off errors.

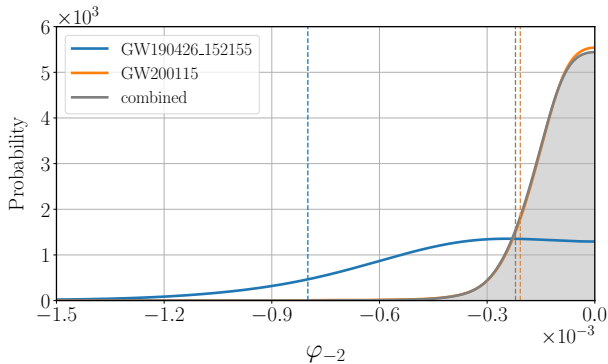


Figure 6. The posterior distribution of φ_{-2} . As mentioned in the main text, we only consider the physically possible prior range, $\varphi_{-2} \leq 0$. The blue and orange colors are used to denote the two events, and the combined result is indicated by the gray color. The dashed vertical lines denote the limits at 90% CL.

work. Since the dipole amplitude depends on the difference between the scalar charges of two components of a binary, If the possibility that the two components have an equal mass cannot be ruled out, we are unable to place an effective constraint. Therefore, we also exclude the two BNS events GW170817 and GW190425 in the analysis.

We place the constraints by performing the full Bayesian inference. The waveform template with the dipole term which is the leading order of modification is used to construct the likelihood. The dipole radiation in scalar-tensor theories is proportional to the square of the scalar charge difference between two component objects of a binary. The scalar charges of black holes are zero which is assured by the no-hair theorem. The scalar charges of neutron stars are gotten by solving TOV equations for BD and DEF. For SMG, the effects of scalar field are expected to be small due to the screening mechanism. So, we adopt a simple assumption that the density of a neutron star is a constant to get the scalar charge.

Four tabular EoS are used when solving TOV equations to get the scalar charges for BD and DEF. However, we do not find the different EoS have significant influences on the results. All results we get are consistent with GR. The constraint on BD is about $\alpha_0 \lesssim 0.1$ or equivalent $\omega_{\text{BD}} \gtrsim 40$. For DEF, we get the constraint $\beta_0 \gtrsim -4.0$. Due to our prior settings and statistical uncertainties, we cannot get the constraints of the parameter $\log_{10} \alpha_0$ in DEF. For SMG, we place the upper limit $\varphi_{\text{VEV}}/M_{\text{Pl}} \lesssim 1.8 \times 10^{-2}$. All constraints presented above are at 90%. The constraint on β_0 in DEF is comparable with the previous constraint from pulsar timing

experiments. The constraints on BD and SMG have no competition with previous constraints given by the solar system tests and pulsar timing experiments. Although the results of this work do not find any new phenomena or push the current constraints to be more stringent, our results complement the tests on these three specific models in the strong-field regime and make preparations for future more NSBH events.

ACKNOWLEDGMENTS

R.N. thanks Yifan Wang for helpful discussions. This work is supported by NSFC No.11773028, 11633001, 11653002, 11603020, 11903030, 12003029, 11903033, the Fundamental Research Funds for the Central Universities under Grant No.WK2030000036, WK344000004 and WK2030000044, the Strategic Priority Research Program of the Chinese Academy of Sciences Grant No. XDB23010200, Key Research Program of the Chinese Academy of Sciences, Grant No. XDPB15, and the China Manned Space Program through its Space Application System, and the China Postdoctoral Science Foundation grant No.2019M662168. This research has made use of data, software and/or web tools obtained from the Gravitational Wave Open Science Center (<https://www.gw-openscience.org/>), a service of LIGO Laboratory, the LIGO Scientific Collaboration and the Virgo Collaboration. LIGO Laboratory and Advanced LIGO are funded by the United States National Science Foundation (NSF) as well as the Science and Technology Facilities Council (STFC) of the United Kingdom, the Max-Planck-Society (MPS), and the State of Niedersachsen/Germany for support of the construction of Advanced LIGO and construction and operation of the GEO600 detector. Additional support for Advanced LIGO was provided by the Australian Research Council. Virgo is funded, through the European Gravitational Observatory (EGO), by the French Centre National de Recherche Scientifique (CNRS), the Italian Istituto Nazionale di Fisica Nucleare (INFN) and the Dutch Nikhef, with contributions by institutions from Belgium, Germany, Greece, Hungary, Ireland, Japan, Monaco, Poland, Portugal, Spain.

Facilities: LIGO, Virgo

Software: Bilby(Ashton et al. 2019), Dynesty(Speagle 2020), LALSuite(LIGO Scientific Collaboration 2018), PESummary(Hoy & Raymond 2020), NumPy(Harris et al. 2020; van der Walt et al. 2011), SciPy(Virtanen et al. 2020), matplotlib(Hunter 2007)

APPENDIX

A. DIFFERENTIAL EQUATIONS FOR NEUTRON STAR STRUCTURE

The scalar charge of a neutron star can be got by solving the TOV equations. The TOV equations for a neutron star in scalar-tensor theories can be found in previous works (Damour & Esposito-Farèse 1993, 1996). We present a succinct summary here for the convenience of reference. Assuming that the neutron star is isolated and nonrotating, the geometry part can be given by the static spherically symmetric metric

$$\begin{aligned} ds_*^2 &= g_{\mu\nu}^* dx^\mu dx^\nu \\ &= -e^{\nu(r)} dt^2 + \frac{dr^2}{1 - 2\mu(r)/r} + r^2(d\theta^2 + \sin^2\theta d\varphi^2). \end{aligned} \quad (\text{A1})$$

The matter part is described by the perfect-fluid form of energy-momentum tensor in Jordan frame

$$\tilde{T}^{\mu\nu} = (\tilde{\rho} + \tilde{p})\tilde{u}^\mu\tilde{u}^\nu + \tilde{p}\tilde{g}^{\mu\nu}. \quad (\text{A2})$$

We use tilde to denote a quantity in the Jordan frame and star to denote a quantity in the Einstein frame. \tilde{T} and T_* are related by $T_* = A^4(\varphi)\tilde{T}$. Taking the above metric (A1) and energy-momentum tensor (A2) into the field equations (2) and energy-momentum conservation equation $\tilde{\nabla}_\mu\tilde{T}^{\mu\nu} = 0$, one can get the following differential equations, which describe the structure of neutron star,

$$\begin{aligned} \mu' &= 4\pi G_* r^2 A^4(\varphi)\tilde{\rho} + \frac{1}{2}r(r - 2\mu)\psi^2 \\ \nu' &= 8\pi G_* A^4(\varphi)\frac{r^2}{r - 2\mu}\tilde{p} + r\psi^2 + \frac{2\mu}{r(r - 2\mu)} \\ \varphi' &= \psi \\ \psi' &= 4\pi G_* A^4(\varphi)\frac{r}{r - 2\mu} [\alpha(\varphi)(\tilde{\rho} - 3\tilde{p}) + r\psi(\tilde{\rho} - \tilde{p}) \\ &\quad - \frac{2(r - \mu)}{r(r - 2\mu)}\psi] \\ \tilde{p}' &= -(\tilde{\rho} - \tilde{p}) \left[4\pi G_* \frac{r^2 A^4(\varphi)\tilde{p}}{r - 2\mu} + \frac{1}{2}r\psi^2 + \frac{\mu}{r(r - 2\mu)} \right. \\ &\quad \left. + \alpha(\varphi)\psi \right]. \end{aligned} \quad (\text{A3})$$

The above equations can be solved once the EoS, which is the relation between $\tilde{\rho}$ and \tilde{p} , and the initial conditions are given. Physical quantities, the scalar charge, the scalar field at infinity and the gravitational mass, can be extracted from the solution by matching the interior and exterior solutions,

$$\alpha_A = -\frac{2\psi_s}{\nu'_s} \quad (\text{A4})$$

$$\varphi_0 = \varphi_s + \frac{2\psi_s}{(\nu_s'^2 + 4\psi_s^2)^{1/2}} \operatorname{arctanh} \left[\frac{(\nu_s'^2 + 4\psi_s^2)^{1/2}}{\nu'_s + 2/r_s} \right] \quad (\text{A5})$$

$$m_A = \frac{r_s^2 \nu'_s}{2G_*} \left(1 - \frac{2\mu_s}{r_s} \right)^{1/2} \exp \left[-\frac{\nu'_s}{(\nu_s'^2 + 4\psi_s^2)^{1/2}} \operatorname{arctanh} \left(\frac{(\nu_s'^2 + 4\psi_s^2)^{1/2}}{\nu'_s + 2/r_s} \right) \right] \quad (\text{A6})$$

where the subscribe s denotes that the quantities take the values at the star surface.

B. POSTERIOR DISTRIBUTION OF OTHER PARAMETERS

In order to verify the reliability of our sampling, we compare our results with the posterior data released by LVC⁷. We select one of our multiple runs for each event as an example to plot together with parameter estimation samples in the posterior data files released by LVC in Figure 7 and Figure 8. The posterior distributions of some interior parameters and the luminosity distance are presented by the corner plot.

The definitions and labels of the parameters follow the conventions implemented in `bilby`. The blue lines and regions denote our results and the red for the results from LVC. The dashed vertical lines represent the 5% and 95% quantiles. Since we make our discussion based on the assumption that the secondary of GW190426_152155 is a neutron star and impose a constraint $m_2 \in [1.0, 2.0]$, the result of mass ratio has slight differences with the result from LVC. Due to the degeneracy between aligned spin and mass ratio, the result of effective inspiral spin parameter has also a little mismatch with LVC result. Except this, the sampling results of other parameters are consistent with the results released by LVC quite well.

All results of our parameter estimation can be found on Zenodo⁸. The differences between all our results and LVC's are within tolerance.

C. COMPARISON OF THE CONSTRAINTS ON DIPOLE RADIATION

As discussed in Section 3, it has practical difficult to constrain α_0 or (α_0, β_0) by the events GW170817 and GW190425. However, these two events can be used to constrain the dipole radiation without considering specific model parameters. In order to compare the results given by LVC, we also perform the tests on φ_{-2} for these two events. We follow the method of model-independent parameterized tests used by LVC (Abbott et al. 2019a; Collaboration et al. 2020; Abbott et al. 2016a, 2019b), except that we only consider the physical range of $\varphi_{-2} < 0$ which represents the positive outgoing energy flux. Following the works of LVC (Abbott et al. 2020a, 2019c), we use the pre-processed data in which the glitches have been subtracted (Driggers et al. 2019; Cornish & Littenberg 2015; Davis et al. 2019; Pankow et al. 2018; LVC 2017, 2018, 2019a) and event-specific PSDs encapsulated in LVC posterior sample releases (LVC 2020b, 2019b) to perform full Bayesian inference.

The results are shown in Figure 9. The limits at 90% CL are shown by the dashed vertical lines. The limit for GW170817 is about 10^{-5} which is consistent with the result reported by LVC (Abbott et al. 2019b). The limit provided by GW190425 is comparable with GW170817, only have a slight difference within the same order of magnitude. While the limits given by the two NSBH events are much worse than the limits given by the two BNS events. The better constraint is because the BNS events has a lighter mass which allows more circles of inspiral to be observed in the detectors sensitive band. Due to the same reason, the limit given by GW200115 is slightly better than limit given by GW190426_152155.

D. RELATIONS BETWEEN THE SCALAR CHARGE AND THE MASS FOR DIFFERENT EOS

The EoS has to be given in order to solve the TOV equation. Considering the measurements of the millisecond pulsar PSR J0030+0451 and PSR J0740+6620 (Miller et al. 2019; Riley et al. 2019; Miller et al. 2021; Riley et al. 2021) and observation evidence that the maximum mass of neutron stars can exceed $2M_\odot$ (Antoniadis et al. 2013; Cromartie et al. 2019; Demorest et al. 2010; Fonseca et al. 2016; Arzoumanian et al. 2018), we select four commonly used EoS, `sly`, `alf2`, `H4` and `mpa1` in this work. We illustrate the relations between mass and radius in GR of these EoS⁹ and the measurements of pulsar mass and radius form two independent groups in Figure 10. The four solid lines represent the EoS used in this work, and the translucent error bars indicate the 68% credible regions of mass-radius measurements.

Using the four EoS, we can solve the TOV equations by the process discussed in Section 2 and extract the scalar charges and mass from the solutions by the equations (A4). The relations between the mass and the scalar charge are shown in Figure 11 for BD and Figure 12 for DEF. For BD, as can be seen in Figure 11, the influence of using different EoS is slight. The differences of the scalar charge (relative to α_0) are within the order of 0.1. Unlike BD, the curves represent the relation between scalar charge and mass have apparent differences for different EoS in DEF. The same conclusion also was presented in previous works (Shao et al. 2017; Shibata et al. 2014). For different EoS,

⁷ <https://dcc.ligo.org/LIGO-P2100143/public> for GW200115 and <https://dcc.ligo.org/LIGO-P2000223/public> for GW190426_152155

⁸ <https://doi.org/10.5281/zenodo.5188445>

⁹ data used to plot are downloaded from http://xtreme.as.arizona.edu/NeutronStars/data/mr_tables.tar

GW190426_152155

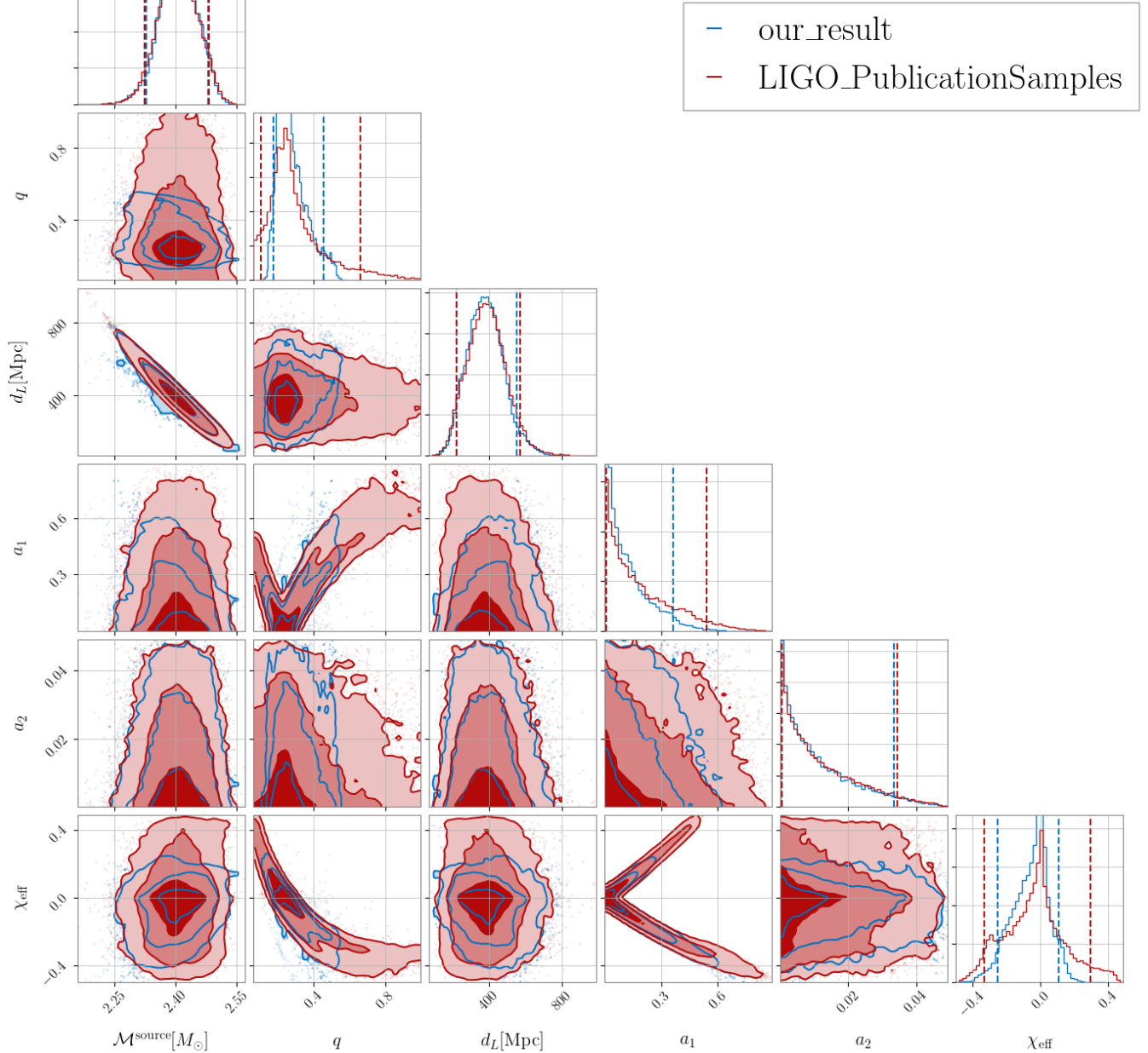


Figure 7. Comparison between our sampling results and posterior samples released by LVC for the event GW190426_152155. The blue regions and lines denote our results and the red for LVC. The dashed vertical lines denote the 5% and 95% quantiles. The labels of parameters follow the conventions in `bilby`. Since we impose a constraint on the prior of the secondary mass, the distribution of mass ratio and effective inspiral spin parameter have slight differences with LVC. Our sampling results are consistent with the results released by LVC within tolerance.

1023 the magnitude of scalar charges amplified by scalarization phenomena is almost same, but the scalarization windows
 1024 which is the mass range where the nonperturbative strong-field effects can occur are different.

GW200115

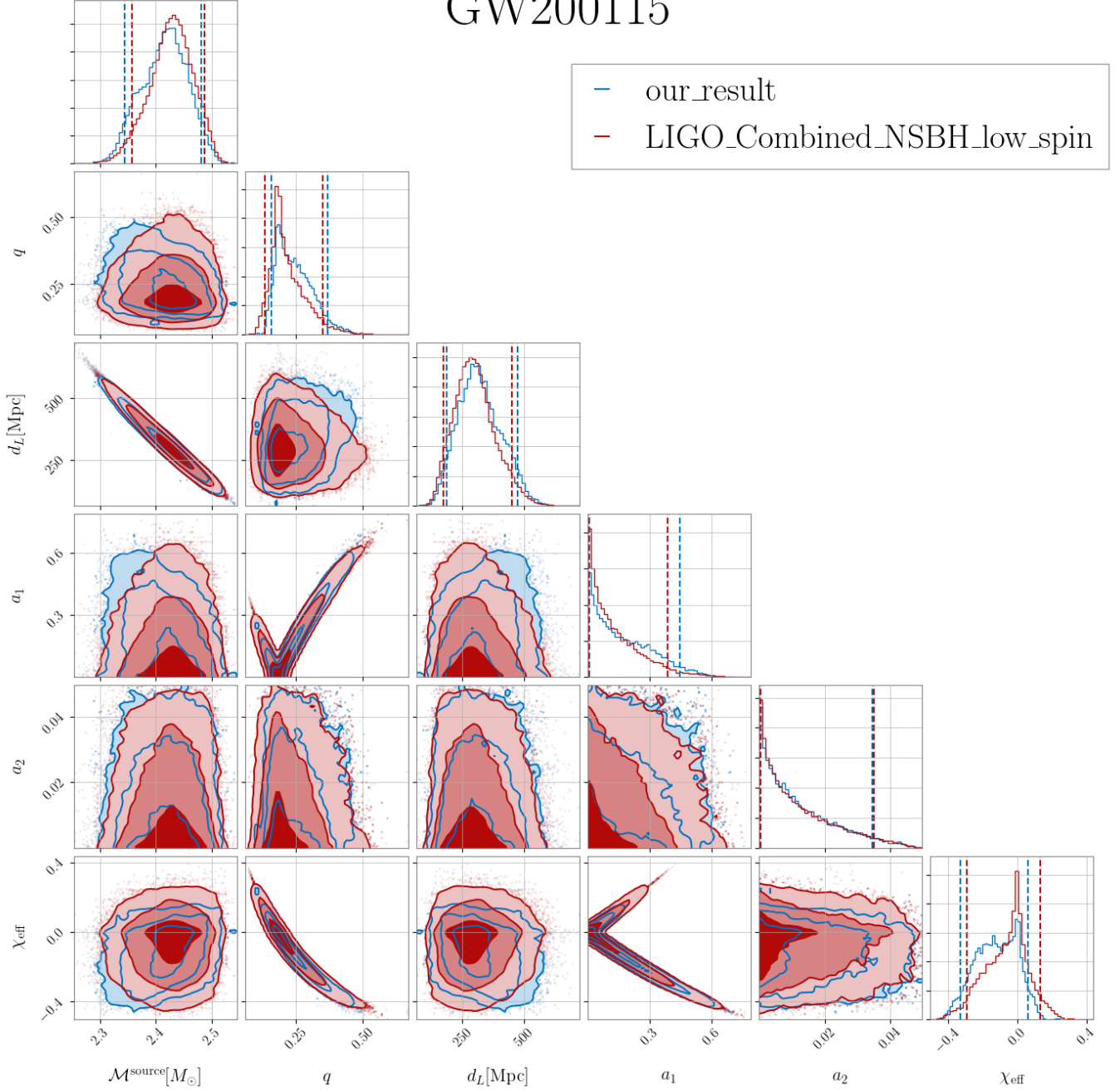


Figure 8. Comparison between our sampling results and posterior samples released by LVC for the event **GW200115**. Keeping the same with the last figure, the blue and red colors are used to denote our results and LVC's, and dashed vertical lines indicate the intervals of 90% CL. The posteriors of GR parameters of the event GW200115 in our runs are also consistent with the results released by LVC within tolerance.

1025

E. UNPHYSICAL DEVIATIONS OF HIGHLY ASYMMETRIC SOURCES

1026 In the main body, we exclude the two events GW190814 and GW200105 due to unphysical deviations. Here, we
 1027 show the posteriors of the dipole modification parameter for these two events in Figure 13 and present more discussion
 1028 below.

1029 Subdominant spherical harmonic multipoles will become important when the mass ratio of sources is large. There
 1030 is strong evidence for the presence of higher modes (HMs) in the analysis of GW190814 (Abbott et al. 2020d).

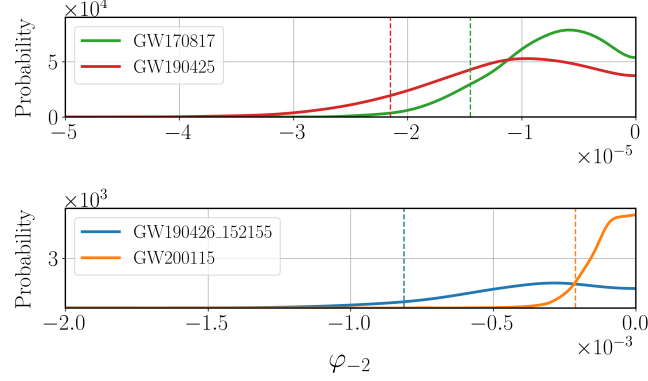


Figure 9. Comparisons between the posterior distributions of φ_{-2} . The dashed vertical lines denote the limits at 90% CL. The limit for GW170817 is about 10^{-5} which is consistent with the result reported by LVC (Abbott et al. 2019b). The limit provided by GW190425 is comparable with GW170817, only have a slight difference within the same order of magnitude. While the limits given by two NSBH events considered in this work are much worse than the limits given by the BNS events. The better constraints are because the BNS events have lighter masses which allows more circles of inspiral to be observed in the detectors sensitive band.

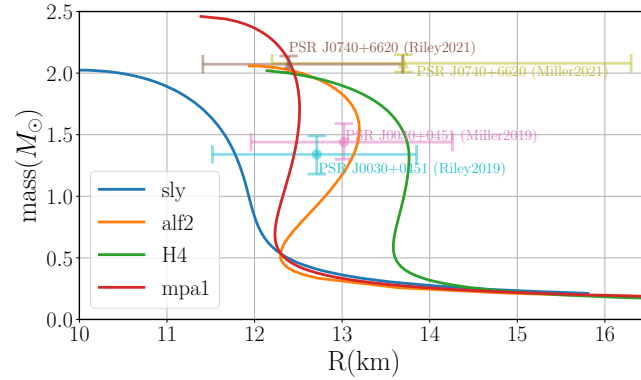


Figure 10. The relation between mass and radius in GR for four EoS used in this work. The four solid lines denote the different EoS, and the translucent error bars denote the 68% credible regions of mass-radius measurements of the millisecond pulsar PSR J0030+0451 and PSR J0740+6620. The pink one indicates the result reported in (Miller et al. 2019) and the cyan is for the result given by (Riley et al. 2019). The brown and olive are denote the most recent results of PSR J0740+6620 from (Riley et al. 2021) and (Miller et al. 2021) respectively. We select this four EoS by considering these observation constraints on mass-radius relation and the observation evidence that the mass of a neutron star can exceed $2M_{\odot}$ (Antoniadis et al. 2013; Cromartie et al. 2019; Demorest et al. 2010; Fonseca et al. 2016; Arzoumanian et al. 2018).

1031 Therefore, following the paper of LVC (Collaboration et al. 2020), we also employ the waveform model incorporating
 1032 HMs, IMRPhenomPv3HM (Khan et al. 2020). The waveform model IMRPhenomPv3HM is based on the model IMRPhenomD
 1033 (Husa et al. 2016; Khan et al. 2016) which is employed in the main body, but incorporates the processing due to the
 1034 in-plane spins and HMs (London et al. 2018; Khan et al. 2019, 2020). Same to LVC (Collaboration et al. 2020), we
 1035 only add the dipole modification on the dominant mode. The non-GR deformation on HMs is gotten by rescaling the
 1036 modification in the dominant mode according to the method presented in (London et al. 2018). There are no new
 1037 coefficients introduced. It is worth to be noted that this method of implementation can possibly be one of the reasons
 1038 that cause the unphysical deviation.

1039 Using this waveform model, we perform the same Bayesian inference discussed in the main body on the two events
 1040 GW190814 and GW200105 to constrain the dipole modification parameter φ_{-2} . The results are shown in Figure 13.
 1041 The dashed vertical lines indicate 5% and 95% percentiles for the two events respectively. It can be seen that the GR
 1042 value falls in the tails of the posteriors and is excluded from the intervals of 90% CL for these two events. The best

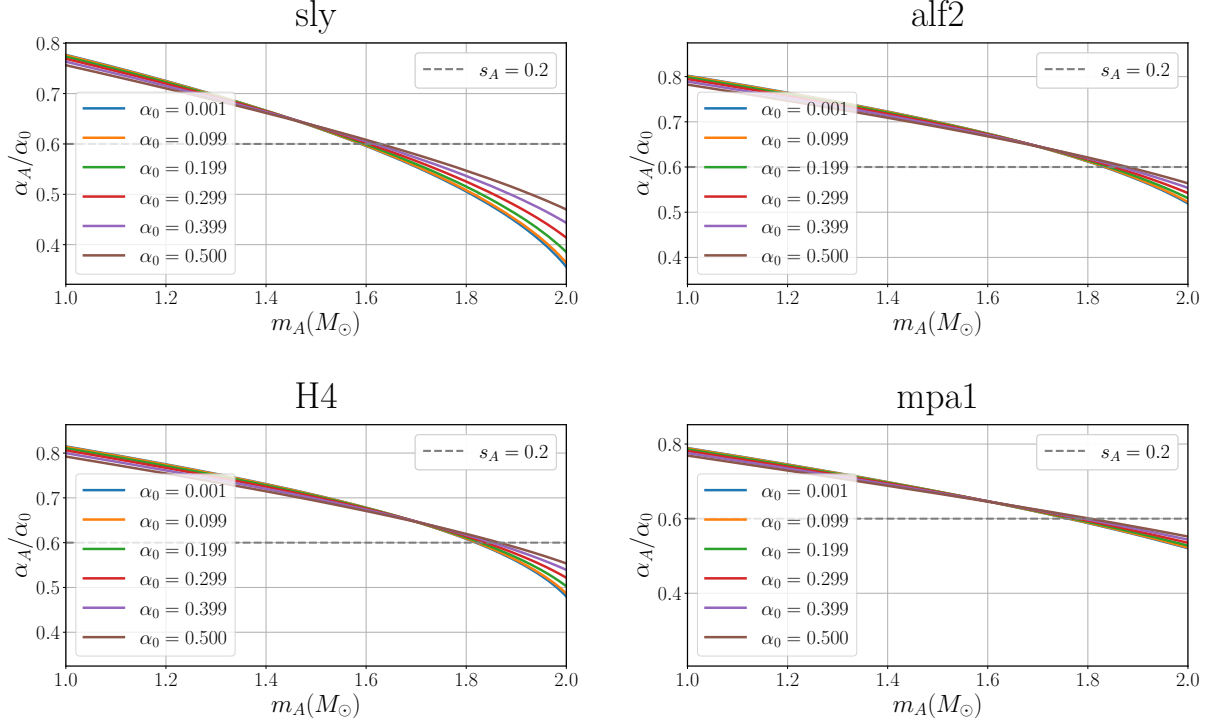


Figure 11. The relation between scalar charge and mass in BD for four different EoS. Different colors are used to denote different values of α_0 . These results show the relation is similar for different EoS in BD. The differences of the scalar charge (relative to α_0) are within the order of 0.1.

fit value of GW190814 deviates from the GR value in the order of 10^{-3} . While the deviation of GW200105 is slightly reduced. The result of GW190814 presented here is consistent with the result of LVC (as can be seen in Figure 19 of (Collaboration et al. 2020)). Similar deviations are also reported in (Perkins et al. 2021). These results are believed to be not the real deviations from GR. The possible reasons for these deviations might be the systematic errors of the waveform templates or the parameterization method of non-GR modification (which might be inappropriate when HMs are present as pointed out above), and covariances between model parameters (Collaboration et al. 2020; Perkins et al. 2021).

We also find the deviations are somehow related to the mass parameters of sources. Referring to Figure 4 in (Abbott et al. 2021a), We also illustrate the component masses of all 4 possible NSBH events so far in Figure 14. The 90% CL regions of the joint posterior distribution for component masses are enclosed by the solid curves, and the shading denotes the posterior probability. The dashed gray lines indicate the constant mass ratio. The posterior distributions of GW190426_152155 and GW200115 are almost overlapped. The posteriors of these two events are the most dispersed and have more part in the lower mass ratio. Meanwhile, the deviations on φ_{-2} are absent for these two events. The events GW190814 and GW200105 have higher mass ratio, and the magnitude of deviation from GR value is consistent with their mass ratio as can be observed by combining Figures 14 and 13.

For the sources with large mass ratio, the HMs becomes more important which may complicate the analysis. As discussed above, the non-GR modifications on HMs are propagated from the rescalings of the modifications on the dominant mode according to the rules presented in (London et al. 2018). The rescaling rules are verified for the GR part by numerical relativity but are doubtful for the non-GR part. The method of performing the parameterized tests may be inapplicable when HMs are present. The parameterized tests have not been systematically studied in the parameter space of highly asymmetric sources. More thorough studies are needed to explain these deviations. In this work, we simply exclude the two events GW190814 and GW200105.

REFERENCES

- Abbott, B., Abbott, R., Abbott, T., et al. 2016a, Physical Review Letters, 116, 221101, doi: 10.1103/physrevlett.116.221101
- , 2016b, Physical Review Letters, 116, 061102, doi: 10.1103/physrevlett.116.061102

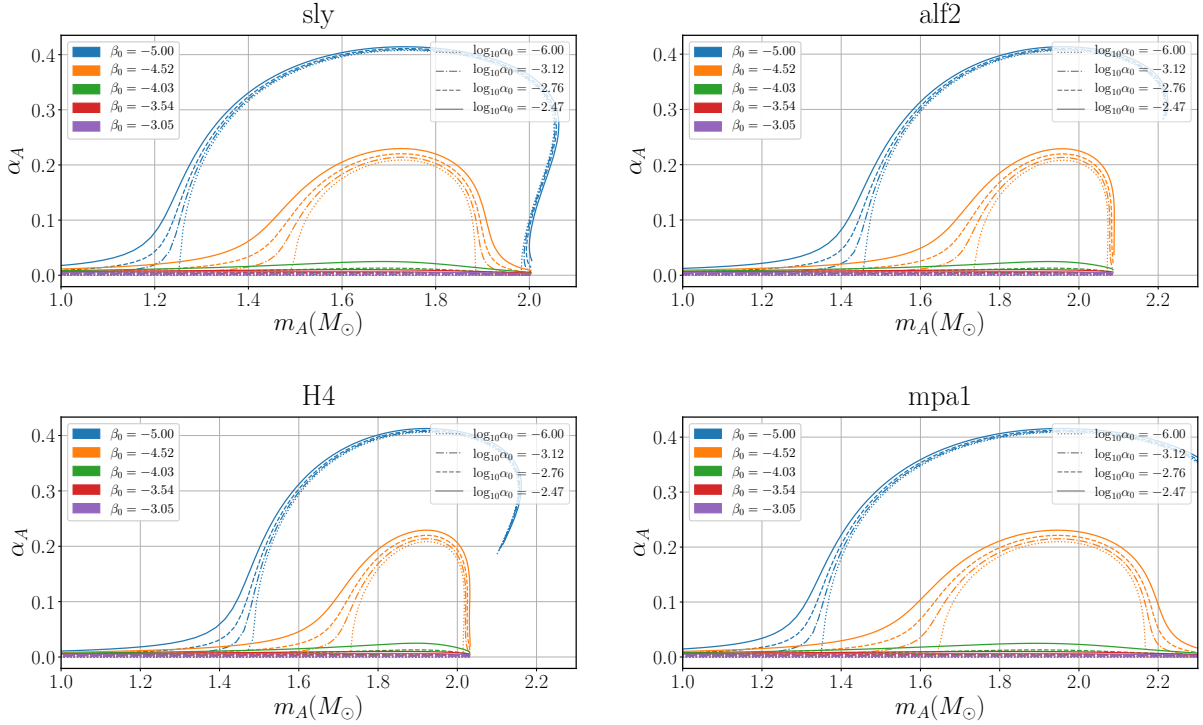


Figure 12. The relation between scalar charge and mass in DEF for four different EoS. The colors are used to denote the values of β_0 and the line styles are used to denote the values of α_0 . For different EoS, the magnitude of scalar charges amplified by scalarization phenomena is almost same, but the scalarization windows which is the mass range where the nonperturbative strong-field effects can occur are different.

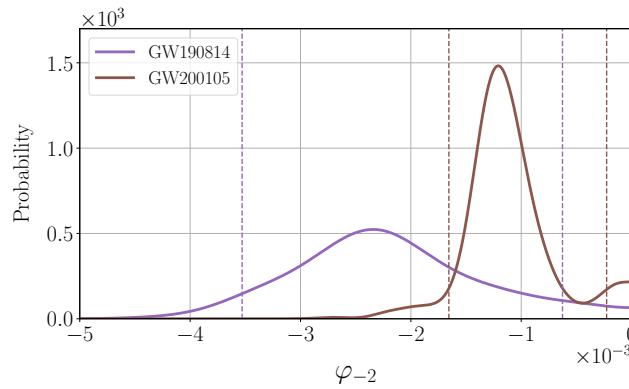


Figure 13. The posteriors of the dipole modification parameter φ_{-2} for the two NSBH events excluded in this work. The dashed vertical lines indicate 5% and 95% percentiles for the two events respectively. In the posterior of GW190814, the best fit value deviates from the GR value in the order of 10^{-3} , the GR value falls in the tail and is excluded from the 90% confidence interval. The deviation shown here is in agreement with the LVC analysis which can be seen in Figure 19 of (Collaboration et al. 2020). The similar deviation is also present in the result of GW200105.

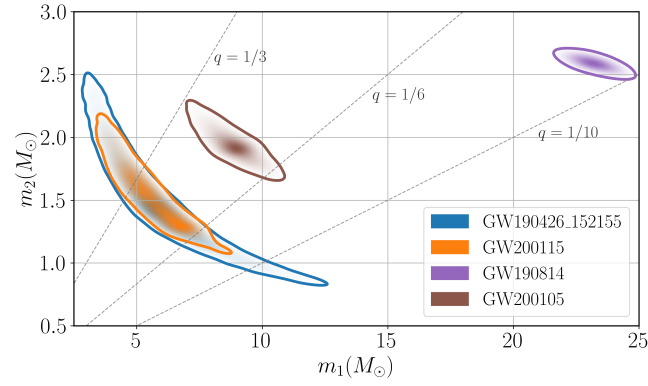


Figure 14. The component masses of all 4 possible NSBH events so far. Following Figure 4 in (Abbott et al. 2021a), we illustrate the component masses of the four possible NSBH events for convenience of reference. The 90% CL regions of the joint posterior distribution for component masses are enclosed by the solid curves, and the shading denotes the posterior probability. The dashed gray lines indicate the constant mass ratio. As can be seen in the figure, the GW190814 is the most asymmetric source. Deviations which might be caused by systematic errors of waveform templates, the parameterization method of non-GR modification, or covariances between model parameters, are present in the posteriors of the dipole modification parameter as shown in Figure 19 in (Collaboration et al. 2020), Figure 10 in (Perkins et al. 2021) and Figure 13 in this paper. Similar deviations are also seen in the case of GW200105, but absent in GW190426_152155 and GW200115, which is probably due to the more dispersed posteriors and more probability on lower mass ratio.

- 1070 —. 2017a, *Physical Review Letters*, 119, 161101,
1071 doi: [10.1103/physrevlett.119.161101](https://doi.org/10.1103/physrevlett.119.161101)
- 1072 —. 2018, *Physical Review Letters*, 121, 161101,
1073 doi: [10.1103/physrevlett.121.161101](https://doi.org/10.1103/physrevlett.121.161101)
- 1074 —. 2019a, *Physical Review X*, 9, 031040,
1075 doi: [10.1103/physrevx.9.031040](https://doi.org/10.1103/physrevx.9.031040)
- 1076 —. 2019b, *Physical Review Letters*, 123, 011102,
1077 doi: [10.1103/physrevlett.123.011102](https://doi.org/10.1103/physrevlett.123.011102)
- 1078 —. 2019c, *Physical Review X*, 9, 011001,
1079 doi: [10.1103/physrevx.9.011001](https://doi.org/10.1103/physrevx.9.011001)
- 1080 —. 2019d, *Physical Review D*, 100, 104036,
1081 doi: [10.1103/physrevd.100.104036](https://doi.org/10.1103/physrevd.100.104036)
- 1082 Abbott, B. P., Abbott, R., Abbott, T. D., et al. 2017b, *The*
1083 *Astrophysical Journal*, 848, L12,
1084 doi: [10.3847/2041-8213/aa91c9](https://doi.org/10.3847/2041-8213/aa91c9)
- 1085 —. 2020a, *The Astrophysical Journal*, 892, L3,
1086 doi: [10.3847/2041-8213/ab75f5](https://doi.org/10.3847/2041-8213/ab75f5)
- 1087 —. 2020b, *Classical and Quantum Gravity*, 37, 055002,
1088 doi: [10.1088/1361-6382/ab685e](https://doi.org/10.1088/1361-6382/ab685e)
- 1089 Abbott, R., Abbott, T. D., Abraham, S., et al. 2020c.
1090 <https://arxiv.org/abs/2010.14527>
- 1091 —. 2020d, *The Astrophysical Journal*, 896, L44,
1092 doi: [10.3847/2041-8213/ab960f](https://doi.org/10.3847/2041-8213/ab960f)
- 1093 —. 2021a, *The Astrophysical Journal Letters*, 915, L5,
1094 doi: [10.3847/2041-8213/ac082e](https://doi.org/10.3847/2041-8213/ac082e)
- 1095 —. 2021b, *SoftwareX*, 13, 100658,
1096 doi: [10.1016/j.softx.2021.100658](https://doi.org/10.1016/j.softx.2021.100658)
- 1097 Adelberger, E. G. 2001, *Classical and Quantum Gravity*,
1098 18, 2397, doi: [10.1088/0264-9381/18/13/302](https://doi.org/10.1088/0264-9381/18/13/302)
- 1099 Agathos, M., Pozzo, W. D., Li, T., et al. 2014, *Physical*
1100 *Review D*, 89, 082001, doi: [10.1103/physrevd.89.082001](https://doi.org/10.1103/physrevd.89.082001)
- 1101 Anderson, D., Freire, P., & Yunes, N. 2019,
1102 doi: [10.1088/1361-6382/ab3a1c](https://doi.org/10.1088/1361-6382/ab3a1c)
- 1103 Antoniadis, J., Freire, P. C. C., Wex, N., et al. 2013,
1104 *Science*, 340, 1233232, doi: [10.1126/science.1233232](https://doi.org/10.1126/science.1233232)
- 1105 Arzoumanian, Z., Brazier, A., Burke-Spolaor, S., et al.
1106 2018, *The Astrophysical Journal Supplement Series*, 235,
1107 37, doi: [10.3847/1538-4365/aab5b0](https://doi.org/10.3847/1538-4365/aab5b0)
- 1108 Ashton, G., Hübner, M., Lasky, P. D., et al. 2019, *The*
1109 *Astrophysical Journal Supplement Series*, 241, 27,
1110 doi: [10.3847/1538-4365/ab06fc](https://doi.org/10.3847/1538-4365/ab06fc)
- 1111 Babichev, E., & Deffayet, C. 2013, *Classical and Quantum*
1112 *Gravity*, 30, 184001,
1113 doi: [10.1088/0264-9381/30/18/184001](https://doi.org/10.1088/0264-9381/30/18/184001)
- 1114 Barausse, E., Palenzuela, C., Ponce, M., & Lehner, L. 2013,
1115 *Physical Review D*, 87, 081506,
1116 doi: [10.1103/physrevd.87.081506](https://doi.org/10.1103/physrevd.87.081506)
- 1117 Barrow, J. D., & ichi Maeda, K. 1990, *Nuclear Physics B*,
1118 341, 294, doi: [10.1016/0550-3213\(90\)90272-f](https://doi.org/10.1016/0550-3213(90)90272-f)
- 1119 Bayes, T. 1763, *Philosophical transactions of the Royal*
1120 *Society of London*, 370,
1121 doi: <https://doi.org/10.1098/rstl.1763.0053>
- 1122 Bekenstein, J. D. 1995, *Physical Review D*, 51, R6608,
1123 doi: [10.1103/physrevd.51.r6608](https://doi.org/10.1103/physrevd.51.r6608)
- 1124 Bertotti, B., Iess, L., & Tortora, P. 2003, *Nature*, 425, 374,
1125 doi: [10.1038/nature01997](https://doi.org/10.1038/nature01997)
- 1126 Brans, C., & Dicke, R. H. 1961, *Physical Review*, 124, 925,
1127 doi: [10.1103/physrev.124.925](https://doi.org/10.1103/physrev.124.925)
- 1128 Brax, P. 2012. <https://arxiv.org/abs/1211.5237>
- 1129 Brax, P., Davis, A. C., & Sakstein, J. 2014, *Classical and*
1130 *Quantum Gravity*, 31, 225001,
1131 doi: [10.1088/0264-9381/31/22/225001](https://doi.org/10.1088/0264-9381/31/22/225001)
- 1132 Brax, P., van de Bruck, C., Davis, A., & Green, A. 2006,
1133 *Physics Letters B*, 633, 441,
1134 doi: [10.1016/j.physletb.2005.12.055](https://doi.org/10.1016/j.physletb.2005.12.055)
- 1135 Broadhurst, T., Diego, J. M., & Smoot, G. F. 2020.
1136 <https://arxiv.org/abs/2006.13219>
- 1137 Broekgaarden, F. S., Berger, E., Neijssel, C. J., et al. 2021.
1138 <https://arxiv.org/abs/2103.02608>
- 1139 Buonanno, A., Iyer, B. R., Ochsner, E., Pan, Y., &
1140 Sathyaprakash, B. S. 2009, *Physical Review D*, 80,
1141 084043, doi: [10.1103/physrevd.80.084043](https://doi.org/10.1103/physrevd.80.084043)
- 1142 Burd, A., & Coley, A. 1991, *Physics Letters B*, 267, 330,
1143 doi: [10.1016/0370-2693\(91\)90941-i](https://doi.org/10.1016/0370-2693(91)90941-i)
- 1144 Burgay, M., D'Amico, N., Possenti, A., et al. 2003, *Nature*,
1145 426, 531, doi: [10.1038/nature02124](https://doi.org/10.1038/nature02124)
- 1146 Burrage, C., & Sakstein, J. 2018, *Living Reviews in*
1147 *Relativity*, 21, doi: [10.1007/s41114-018-0011-x](https://doi.org/10.1007/s41114-018-0011-x)
- 1148 Chandrasekhar, S. 1984, *Journal of Astrophysics and*
1149 *Astronomy*, 5, 3, doi: [10.1007/bf02714967](https://doi.org/10.1007/bf02714967)
- 1150 Clifton, T., Ferreira, P. G., Padilla, A., & Skordis, C. 2012,
1151 *Physics Reports*, 513, 1,
1152 doi: [10.1016/j.physrep.2012.01.001](https://doi.org/10.1016/j.physrep.2012.01.001)
- 1153 Cline, D., ed. 2013, *Sources and Detection of Dark Matter*
1154 *and Dark Energy in the Universe* (Springer Netherlands),
1155 doi: [10.1007/978-94-007-7241-0](https://doi.org/10.1007/978-94-007-7241-0)
- 1156 Cognard, I., Freire, P. C. C., Guillemot, L., et al. 2017, *The*
1157 *Astrophysical Journal*, 844, 128,
1158 doi: [10.3847/1538-4357/aa7bee](https://doi.org/10.3847/1538-4357/aa7bee)
- 1159 Collaboration, T. L. S., the Virgo Collaboration, Abbott,
1160 R., et al. 2020. <https://arxiv.org/abs/2010.14529>
- 1161 Cornish, N. J., & Littenberg, T. B. 2015, *Classical and*
1162 *Quantum Gravity*, 32, 135012,
1163 doi: [10.1088/0264-9381/32/13/135012](https://doi.org/10.1088/0264-9381/32/13/135012)
- 1164 Cromartie, H. T., Fonseca, E., Ransom, S. M., et al. 2019,
1165 *Nature Astronomy*, 4, 72, doi: [10.1038/s41550-019-0880-2](https://doi.org/10.1038/s41550-019-0880-2)
- 1166 Cutler, C., & Flanagan, É. E. 1994, *Physical Review D*, 49,
1167 2658, doi: [10.1103/physrevd.49.2658](https://doi.org/10.1103/physrevd.49.2658)
- 1168 Damour, T. 2007. <https://arxiv.org/abs/0704.0749>

- 1169 Damour, T., & Esposito-Farese, G. 1992, *Classical and*
 1170 *Quantum Gravity*, 9, 2093,
 1171 doi: [10.1088/0264-9381/9/9/015](https://doi.org/10.1088/0264-9381/9/9/015)
- 1172 Damour, T., & Esposito-Farèse, G. 1993, *Physical Review*
 1173 *Letters*, 70, 2220, doi: [10.1103/physrevlett.70.2220](https://doi.org/10.1103/physrevlett.70.2220)
 1174 —. 1996, *Physical Review D*, 54, 1474,
 1175 doi: [10.1103/physrevd.54.1474](https://doi.org/10.1103/physrevd.54.1474)
 1176 —. 1998, *Physical Review D*, 58, 042001,
 1177 doi: [10.1103/physrevd.58.042001](https://doi.org/10.1103/physrevd.58.042001)
- 1178 Davis, D., Massinger, T., Lundgren, A., et al. 2019,
 1179 *Classical and Quantum Gravity*, 36, 055011,
 1180 doi: [10.1088/1361-6382/ab01c5](https://doi.org/10.1088/1361-6382/ab01c5)
- 1181 Demorest, P. B., Pennucci, T., Ransom, S. M., Roberts, M.
 1182 S. E., & Hessels, J. W. T. 2010, *Nature*, 467, 1081,
 1183 doi: [10.1038/nature09466](https://doi.org/10.1038/nature09466)
- 1184 DeWitt, B. S. 1967, *Physical Review*, 160, 1113,
 1185 doi: [10.1103/physrev.160.1113](https://doi.org/10.1103/physrev.160.1113)
- 1186 Dietrich, T., Samajdar, A., Khan, S., et al. 2019, *Phys. Rev.*
 1187 *D* 100, 044003 (2019), doi: [10.1103/PhysRevD.100.044003](https://doi.org/10.1103/PhysRevD.100.044003)
- 1188 Driggers, J., Vitale, S., Lundgren, A., et al. 2019, *Physical*
 1189 *Review D*, 99, 042001, doi: [10.1103/physrevd.99.042001](https://doi.org/10.1103/physrevd.99.042001)
- 1190 Esposito-Farese, G. 2004, *AIP Conference Proceedings* 736
 1191 (2004) 35-52, doi: [10.1063/1.1835173](https://doi.org/10.1063/1.1835173)
- 1192 Fierz, M. 1956, *Helv. Phys. Acta*, 29, 128
- 1193 Fonseca, E., Pennucci, T. T., Ellis, J. A., et al. 2016, *The*
 1194 *Astrophysical Journal*, 832, 167,
 1195 doi: [10.3847/0004-637x/832/2/167](https://doi.org/10.3847/0004-637x/832/2/167)
- 1196 Freire, P. C. C., Wex, N., Esposito-Farèse, G., et al. 2012,
 1197 *Monthly Notices of the Royal Astronomical Society*, 423,
 1198 3328, doi: [10.1111/j.1365-2966.2012.21253.x](https://doi.org/10.1111/j.1365-2966.2012.21253.x)
- 1199 Harris, C. R., Millman, K. J., van der Walt, S. J., et al.
 1200 2020, *Nature*, 585, 357, doi: [10.1038/s41586-020-2649-2](https://doi.org/10.1038/s41586-020-2649-2)
- 1201 Hastings, W. K. 1970, *Biometrika*, 57, 97,
 1202 doi: [10.1093/biomet/57.1.97](https://doi.org/10.1093/biomet/57.1.97)
- 1203 Hawking, S. W. 1972, *Communications in Mathematical*
 1204 *Physics*, 25, 167, doi: [10.1007/bf01877518](https://doi.org/10.1007/bf01877518)
- 1205 Hinterbichler, K., & Khoury, J. 2010, *Physical Review*
 1206 *Letters*, 104, 231301, doi: [10.1103/physrevlett.104.231301](https://doi.org/10.1103/physrevlett.104.231301)
- 1207 Hofmann, F., Müller, J., & Biskupek, L. 2010, *Astronomy &*
 1208 *Astrophysics*, 522, L5, doi: [10.1051/0004-6361/201015659](https://doi.org/10.1051/0004-6361/201015659)
- 1209 Hoy, C., & Raymond, V. 2020.
 1210 <https://arxiv.org/abs/2006.06639>
- 1211 Hoyle, C. D., Schmidt, U., Heckel, B. R., et al. 2001,
 1212 *Physical Review Letters*, 86, 1418,
 1213 doi: [10.1103/physrevlett.86.1418](https://doi.org/10.1103/physrevlett.86.1418)
- 1214 Hunter, J. D. 2007, *Computing in Science & Engineering*, 9,
 1215 90, doi: [10.1109/mcse.2007.55](https://doi.org/10.1109/mcse.2007.55)
- 1216 Husa, S., Khan, S., Hannam, M., et al. 2016, *Physical*
 1217 *Review D*, 93, 044006, doi: [10.1103/physrevd.93.044006](https://doi.org/10.1103/physrevd.93.044006)
- 1218 Ishak, M. 2018, *Living Reviews in Relativity*, 22,
 1219 doi: [10.1007/s41114-018-0017-4](https://doi.org/10.1007/s41114-018-0017-4)
- 1220 Jain, B., & Khoury, J. 2010, *Annals of Physics*, 325, 1479,
 1221 doi: [10.1016/j.aop.2010.04.002](https://doi.org/10.1016/j.aop.2010.04.002)
- 1222 Jordan, P. 1955, *Schwerkraft und Weltall: Grundlagen d.*
 1223 *theoret. Kosmologie. Mit 13 Abb (Vieweg)*
- 1224 Joyce, A., Jain, B., Khoury, J., & Trodden, M. 2015,
 1225 *Physics Reports*, 568, 1,
 1226 doi: [10.1016/j.physrep.2014.12.002](https://doi.org/10.1016/j.physrep.2014.12.002)
- 1227 Kainulainen, K., & Sunhede, D. 2006, *Physical Review D*,
 1228 73, 083510, doi: [10.1103/physrevd.73.083510](https://doi.org/10.1103/physrevd.73.083510)
- 1229 Kaluza, T. 1921, *Sitzungsberichte der Königlich*
 1230 *Preußischen Akademie der Wissenschaften (Berlin, 966*
 1231 *Khan, S., Chatziioannou, K., Hannam, M., & Ohme, F.*
 1232 2019, *Physical Review D*, 100, 024059,
 1233 doi: [10.1103/physrevd.100.024059](https://doi.org/10.1103/physrevd.100.024059)
- 1234 Khan, S., Husa, S., Hannam, M., et al. 2016, *Physical*
 1235 *Review D*, 93, 044007, doi: [10.1103/physrevd.93.044007](https://doi.org/10.1103/physrevd.93.044007)
- 1236 Khan, S., Ohme, F., Chatziioannou, K., & Hannam, M.
 1237 2020, *Physical Review D*, 101, 024056,
 1238 doi: [10.1103/physrevd.101.024056](https://doi.org/10.1103/physrevd.101.024056)
- 1239 Khoury, J. 2010. <https://arxiv.org/abs/1011.5909>
- 1240 Khoury, J., & Weltman, A. 2004a, *Physical Review D*, 69,
 1241 044026, doi: [10.1103/physrevd.69.044026](https://doi.org/10.1103/physrevd.69.044026)
- 1242 —. 2004b, *Physical Review Letters*, 93, 171104,
 1243 doi: [10.1103/physrevlett.93.171104](https://doi.org/10.1103/physrevlett.93.171104)
- 1244 Kiefer, C. 2007, in *Approaches to Fundamental Physics*
 1245 (Springer Berlin Heidelberg), 123–130,
 1246 doi: [10.1007/978-3-540-71117-9_7](https://doi.org/10.1007/978-3-540-71117-9_7)
- 1247 Klein, O. 1926, *Zeitschrift fur Physik*, 37, 895,
 1248 doi: [10.1007/bf01397481](https://doi.org/10.1007/bf01397481)
- 1249 Koyama, K. 2016, *Reports on Progress in Physics*, 79,
 1250 046902, doi: [10.1088/0034-4885/79/4/046902](https://doi.org/10.1088/0034-4885/79/4/046902)
- 1251 Kramer, M. 2017, in *The Fourteenth Marcel Grossmann*
 1252 *Meeting (WORLD SCIENTIFIC)*,
 1253 doi: [10.1142/9789813226609_0006](https://doi.org/10.1142/9789813226609_0006)
- 1254 Li, Y.-J., Han, M.-Z., Tang, S.-P., et al. 2020.
 1255 <https://arxiv.org/abs/2012.04978>
- 1256 LIGO Scientific Collaboration. 2018, *LIGO Algorithm*
 1257 *Library - LALSuite, free software (GPL)*,
 1258 doi: [10.7935/GT1W-FZ16](https://doi.org/10.7935/GT1W-FZ16)
- 1259 LIGO Scientific Collaboration and Virgo Collaboration.
 1260 2020, *LIGO Virgo strain data from GW200115 event*,
 1261 *Gravitational Wave Open Science Center*,
 1262 doi: [10.7935/KM62-2436](https://doi.org/10.7935/KM62-2436)
- 1263 Littenberg, T. B., & Cornish, N. J. 2015, *Physical Review*
 1264 *D*, 91, 084034, doi: [10.1103/physrevd.91.084034](https://doi.org/10.1103/physrevd.91.084034)
- 1265 Liu, T., Zhang, X., & Zhao, W. 2018a, *Physics Letters B*,
 1266 777, 286, doi: [10.1016/j.physletb.2017.12.051](https://doi.org/10.1016/j.physletb.2017.12.051)

- 1267 Liu, T., Zhao, W., & Wang, Y. 2020, *Physical Review D*,
1268 102, 124035, doi: [10.1103/physrevd.102.124035](https://doi.org/10.1103/physrevd.102.124035)
- 1269 Liu, T., Zhang, X., Zhao, W., et al. 2018b, *Physical Review*
1270 *D*, 98, 083023, doi: [10.1103/physrevd.98.083023](https://doi.org/10.1103/physrevd.98.083023)
- 1271 London, L., Khan, S., Fauchon-Jones, E., et al. 2018,
1272 *Physical Review Letters*, 120, 161102,
1273 doi: [10.1103/physrevlett.120.161102](https://doi.org/10.1103/physrevlett.120.161102)
- 1274 LVC. 2017, Data release for event GW170817.
1275 <https://www.gw-openscience.org/events/GW170817/>
1276 —. 2018, GWTC-1 Documentation.
1277 <https://www.gw-openscience.org/GWTC-1/>
1278 —. 2019a, Glitch model for GW190425.
1279 <https://dcc.ligo.org/LIGO-T1900685/public>
1280 —. 2019b, Power Spectral Densities (PSD) release for
1281 GWTC-1. <https://dcc.ligo.org/LIGO-P1900011/public>
1282 —. 2020a, GWTC-2 Data Release: Parameter Estimation
1283 Samples and Skymaps.
1284 <https://dcc.ligo.org/LIGO-P2000223/public>
1285 —. 2020b, Parameter estimation sample release for
1286 GW190425. <https://dcc.ligo.org/LIGO-P2000026/public>
- 1287 Manchester, R. N. 2015, *International Journal of Modern*
1288 *Physics D*, 24, 1530018, doi: [10.1142/s0218271815300189](https://doi.org/10.1142/s0218271815300189)
- 1289 Metropolis, N., Rosenbluth, A. W., Rosenbluth, M. N.,
1290 Teller, A. H., & Teller, E. 1953, *The Journal of Chemical*
1291 *Physics*, 21, 1087, doi: [10.1063/1.1699114](https://doi.org/10.1063/1.1699114)
- 1292 Miller, M. C., Lamb, F. K., Dittmann, A. J., et al. 2019,
1293 *The Astrophysical Journal*, 887, L24,
1294 doi: [10.3847/2041-8213/ab50c5](https://doi.org/10.3847/2041-8213/ab50c5)
- 1295 —. 2021. <https://arxiv.org/abs/2105.06979>
- 1296 Most, E. R., Papenfort, L. J., Weih, L. R., & Rezzolla, L.
1297 2020, *Monthly Notices of the Royal Astronomical*
1298 *Society: Letters*, 499, L82, doi: [10.1093/mnrasl/slaa168](https://doi.org/10.1093/mnrasl/slaa168)
- 1299 Niu, R., Zhang, X., Liu, T., et al. 2020, *The Astrophysical*
1300 *Journal*, 890, 163, doi: [10.3847/1538-4357/ab6d03](https://doi.org/10.3847/1538-4357/ab6d03)
- 1301 Palenzuela, C., Barausse, E., Ponce, M., & Lehner, L. 2014,
1302 *Physical Review D*, 89, 044024,
1303 doi: [10.1103/physrevd.89.044024](https://doi.org/10.1103/physrevd.89.044024)
- 1304 Pankow, C., Chatziioannou, K., Chase, E. A., et al. 2018,
1305 *Physical Review D*, 98, 084016,
1306 doi: [10.1103/physrevd.98.084016](https://doi.org/10.1103/physrevd.98.084016)
- 1307 Perkins, S. E., Nair, R., Silva, H. O., & Yunes, N. 2021.
1308 <https://arxiv.org/abs/2104.11189>
- 1309 Riley, T. E., Watts, A. L., Bogdanov, S., et al. 2019, *The*
1310 *Astrophysical Journal*, 887, L21,
1311 doi: [10.3847/2041-8213/ab481c](https://doi.org/10.3847/2041-8213/ab481c)
- 1312 Riley, T. E., Watts, A. L., Ray, P. S., et al. 2021.
1313 <https://arxiv.org/abs/2105.06980>
- 1314 Romano, J. D., & Cornish, N. J. 2017, *Living Reviews in*
1315 *Relativity*, 20, doi: [10.1007/s41114-017-0004-1](https://doi.org/10.1007/s41114-017-0004-1)
- 1316 Romero-Shaw, I. M., Talbot, C., Biscoveanu, S., et al. 2020,
1317 *Monthly Notices of the Royal Astronomical Society*, 499,
1318 3295, doi: [10.1093/mnras/staa2850](https://doi.org/10.1093/mnras/staa2850)
- 1319 Román-Garza, J., Bavera, S. S., Fragos, T., et al. 2020.
1320 <https://arxiv.org/abs/2012.02274>
- 1321 Sabulsky, D., Dutta, I., Hinds, E., et al. 2019, *Physical*
1322 *Review Letters*, 123, 061102,
1323 doi: [10.1103/physrevlett.123.061102](https://doi.org/10.1103/physrevlett.123.061102)
- 1324 Sahni, V. 2004, in *The Physics of the Early Universe*
1325 (Springer Berlin Heidelberg), 141–179,
1326 doi: [10.1007/978-3-540-31535-3_5](https://doi.org/10.1007/978-3-540-31535-3_5)
- 1327 Sakstein, J. 2020, *Int.J.Mod.Phys. D27* (2018) no.15,
1328 1848008. <https://arxiv.org/abs/2002.04194>
- 1329 Sampson, L., Yunes, N., Cornish, N., et al. 2014, *Physical*
1330 *Review D*, 90, 124091, doi: [10.1103/physrevd.90.124091](https://doi.org/10.1103/physrevd.90.124091)
- 1331 Schimd, C., Uzan, J.-P., & Riazuelo, A. 2005, *Physical*
1332 *Review D*, 71, 083512, doi: [10.1103/physrevd.71.083512](https://doi.org/10.1103/physrevd.71.083512)
- 1333 Shao, L., Sennett, N., Buonanno, A., Kramer, M., & Wex,
1334 N. 2017, *Physical Review X*, 7, 041025,
1335 doi: [10.1103/physrevx.7.041025](https://doi.org/10.1103/physrevx.7.041025)
- 1336 Shibata, M., Taniguchi, K., Okawa, H., & Buonanno, A.
1337 2014, *Physical Review D*, 89, 084005,
1338 doi: [10.1103/physrevd.89.084005](https://doi.org/10.1103/physrevd.89.084005)
- 1339 Skilling, J. 2004, in *AIP Conference Proceedings* (AIP),
1340 doi: [10.1063/1.1835238](https://doi.org/10.1063/1.1835238)
- 1341 Skilling, J. 2006, *Bayesian Analysis*, 1, 833,
1342 doi: [10.1214/06-ba127](https://doi.org/10.1214/06-ba127)
- 1343 Sotiriou, T. P., & Faraoni, V. 2012, *Physical Review*
1344 *Letters*, 108, 081103, doi: [10.1103/physrevlett.108.081103](https://doi.org/10.1103/physrevlett.108.081103)
- 1345 Speagle, J. S. 2020, *Monthly Notices of the Royal*
1346 *Astronomical Society*, 493, 3132,
1347 doi: [10.1093/mnras/staa278](https://doi.org/10.1093/mnras/staa278)
- 1348 Stairs, I. H. 2003, *Living Reviews in Relativity*, 6,
1349 doi: [10.12942/lrr-2003-5](https://doi.org/10.12942/lrr-2003-5)
- 1350 Stovall, K., Freire, P. C. C., Chatterjee, S., et al. 2018, *The*
1351 *Astrophysical Journal*, 854, L22,
1352 doi: [10.3847/2041-8213/aaad06](https://doi.org/10.3847/2041-8213/aaad06)
- 1353 Tahura, S., & Yagi, K. 2018, *Physical Review D*, 98,
1354 084042, doi: [10.1103/physrevd.98.084042](https://doi.org/10.1103/physrevd.98.084042)
- 1355 Vainshtein, A. 1972, *Physics Letters B*, 39, 393,
1356 doi: [10.1016/0370-2693\(72\)90147-5](https://doi.org/10.1016/0370-2693(72)90147-5)
- 1357 van der Walt, S., Colbert, S. C., & Varoquaux, G. 2011,
1358 *Computing in Science & Engineering*, 13, 22,
1359 doi: [10.1109/mcse.2011.37](https://doi.org/10.1109/mcse.2011.37)
- 1360 Virtanen, P., , Gommers, R., et al. 2020, *Nature Methods*,
1361 17, 261, doi: [10.1038/s41592-019-0686-2](https://doi.org/10.1038/s41592-019-0686-2)
- 1362 Wex, N. 2014. <https://arxiv.org/abs/1402.5594>
- 1363 Will, C. M. 1994, *Phys.Rev. D50* (1994) 6058-6067,
1364 doi: [10.1103/PhysRevD.50.6058](https://doi.org/10.1103/PhysRevD.50.6058)

- 1365 —. 2014, *Living Reviews in Relativity*, 17,
1366 doi: [10.12942/lrr-2014-4](https://doi.org/10.12942/lrr-2014-4)
- 1367 —. 2018, *Theory and Experiment in Gravitational Physics*
1368 (Cambridge University Press),
1369 doi: [10.1017/9781316338612](https://doi.org/10.1017/9781316338612)
- 1370 Yasunori Fujii, K.-I. M. 2016, *The Scalar-Tensor Theory of*
1371 *Gravitation* (Cambridge University Press). [https:](https://www.ebook.de/de/product/3876629/yasunori_fujii_kei_ichi_maeda_the_scalar_tensor_theory_of_gravitation.html)
1372 [//www.ebook.de/de/product/3876629/yasunori_fujii_kei_](https://www.ebook.de/de/product/3876629/yasunori_fujii_kei_ichi_maeda_the_scalar_tensor_theory_of_gravitation.html)
1373 [ichi_maeda_the_scalar_tensor_theory_of_gravitation.html](https://www.ebook.de/de/product/3876629/yasunori_fujii_kei_ichi_maeda_the_scalar_tensor_theory_of_gravitation.html)
- 1374 Zhang, X., Liu, T., & Zhao, W. 2017a, *Physical Review D*,
1375 95, 104027, doi: [10.1103/physrevd.95.104027](https://doi.org/10.1103/physrevd.95.104027)
- 1376 Zhang, X., Niu, R., & Zhao, W. 2019a, *Physical Review D*,
1377 100, 024038, doi: [10.1103/physrevd.100.024038](https://doi.org/10.1103/physrevd.100.024038)
- 1378 Zhang, X., Yu, J., Liu, T., Zhao, W., & Wang, A. 2017b,
1379 *Physical Review D*, 95, 124008,
1380 doi: [10.1103/physrevd.95.124008](https://doi.org/10.1103/physrevd.95.124008)
- 1381 Zhang, X., Zhao, W., Huang, H., & Cai, Y. 2016, *Physical*
1382 *Review D*, 93, 124003, doi: [10.1103/physrevd.93.124003](https://doi.org/10.1103/physrevd.93.124003)
- 1383 Zhang, X., Zhao, W., Liu, T., et al. 2019b, *The*
1384 *Astrophysical Journal*, 874, 121,
1385 doi: [10.3847/1538-4357/ab09f4](https://doi.org/10.3847/1538-4357/ab09f4)
- 1386 —. 2019c, *Journal of Cosmology and Astroparticle Physics*,
1387 2019, 019, doi: [10.1088/1475-7516/2019/01/019](https://doi.org/10.1088/1475-7516/2019/01/019)
- 1388 Zhao, J., Shao, L., Cao, Z., & Ma, B.-Q. 2019, *Physical*
1389 *Review D*, 100, 064034, doi: [10.1103/physrevd.100.064034](https://doi.org/10.1103/physrevd.100.064034)
- 1390 Zhao, W., Wright, B. S., & Li, B. 2018, *Journal of*
1391 *Cosmology and Astroparticle Physics*, 2018, 052,
1392 doi: [10.1088/1475-7516/2018/10/052](https://doi.org/10.1088/1475-7516/2018/10/052)